AD-A078 494 JET PROPULSION LAB PASADENA CA F/G 14/2
MONITORING OF LNG VAPORS - PHASE I.(U)
MAR 79 E D HINCKLEY DOT-CG-822868-A
UNCLASSIFIED USCG-D-71-79 NL

1 OF 1
AD-
A 078494

END
DATE
FILMED
1-80
DDC

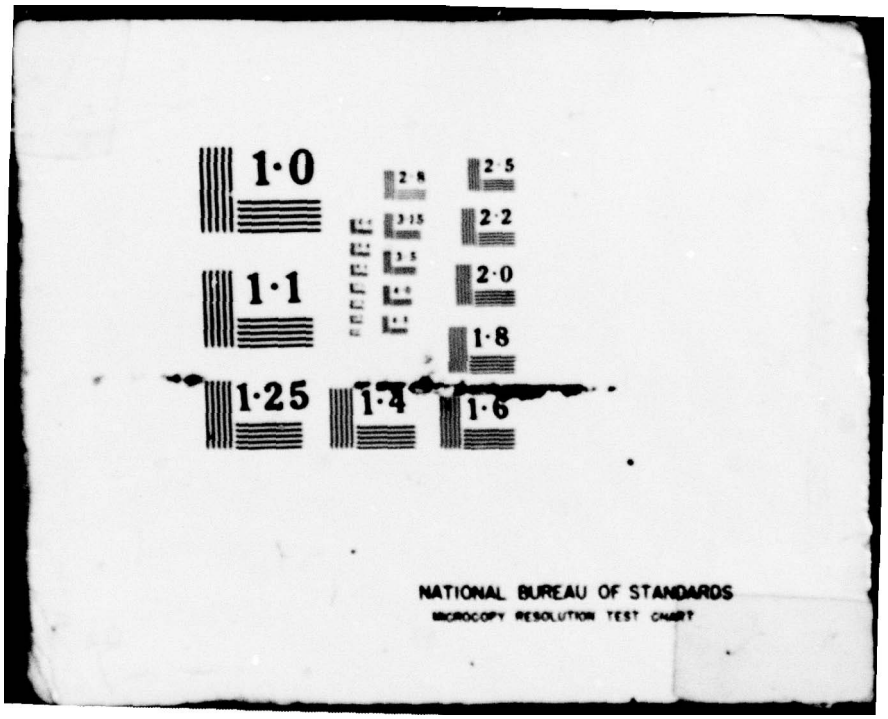
1·0
1·1
1·25
1·4
1·6
2·5
2·2
2·0
1·8
NATIONAL BUREAU OF STANDARDS
MICROCOPY RESOLUTION TEST CHART

Report No. CG-D-71-79

LEVEL II

10

MONITORING OF LNG VAPOR
PHASE I

E. D. HINCKLEY

FINAL REPORT

MARCH 1979

Prepared for

U.S. DEPARTMENT OF TRANSPORTATION
United States Coast Guard
Office of Research and Development
Washington, D.C. 20590

NOTICE

This document is disseminated under the sponsorship of the Department of Transportation in the interest of information exchange. The United States Government assumes no liability for its contents or use thereof.

The contents of this report do not necessarily reflect the official view or policy of the Coast Guard; and they do not constitute a standard, specification, or regulation.

This report, or portions thereof may not be used for advertising or sales promotion purposes. Citation of trade names and manufacturers does not constitute endorsement or approval of such products.

METRIC CONVERSION FACTORS

Approximate Conversions to Metric Measures

Symbol	When You Know	Multiply by	To Find	Symbol
	LENGTH			
	inches	*2.5	centimeters	
	feet	30	centimeters	
	yards	0.9	meters	
	miles	1.6	kilometers	
	AREA			
	square inches	6.5	square centimeters	
	square feet	0.09	square meters	
	square yards	0.8	square meters	
	square miles	2.6	square kilometers	
	acres	0.4	hectares	
	MASS (weight)			
	ounces	28	grams	
	pounds	0.45	kilograms	
	short tons (2000 lb)	0.9	tonnes	
	VOLUME			
	teaspoons	5	milliliters	
	tablespoons	15	milliliters	
	fluid ounces	30	milliliters	
	cups	0.24	liters	
	pints	0.47	liters	
	quarts	0.95	liters	
	gallons	3.8	liters	
	cubic feet	0.03	cubic meters	
	cubic yards	0.76	cubic meters	
	TEMPERATURE (exact)			
°F	Fahrenheit temperature	5/9 (after subtracting 32)	Celsius temperature	°C

*1 in = 2.54 centimeters. For other exact conversions and more detailed tables, see NBS Misc. Publ. 286, Units of Weights and Measures, Price $2.25, SD Catalog No. C13.10:286.

Approximate Conversions from Metric Measures

Symbol	When You Know	Multiply by	To Find	Symbol
	LENGTH			
	millimeters	0.04	inches	
	centimeters	0.4	inches	
	meters	3.3	feet	
	meters	1.1	yards	
	kilometers	0.6	miles	
	AREA			
	square centimeters	0.16	square inches	
	square meters	1.2	square yards	
	square kilometers	0.4	square miles	
	hectares (10,000 m²)	2.5	acres	
	MASS (weight)			
	grams	0.035	ounces	
	kilograms	2.2	pounds	
	tonnes (1000 kg)	1.1	short tons	
	VOLUME			
	milliliters	0.03	fluid ounces	
	liters	2.1	pints	
	liters	1.06	quarts	
	liters	0.26	gallons	
	cubic meters	35	cubic feet	
	cubic meters	1.3	cubic yards	
	TEMPERATURE (exact)			
°C	Celsius temperature	9/5 (then add 32)	Fahrenheit temperature	°F

Technical Report Documentation Page

1. Report No.	2. Government Accession No.	3. Recipient's Catalog No.
USCG-D-71-79		

4. Title and Subtitle	5. Report Date
Monitoring of LNG Vapors - Phase I.	31 MAR 79
	6. Performing Organization Code
	8. Performing Organization Report No.
7. Author(s) E. D. HINCKLEY	
9. Performing Organization Name and Address Jet Propulsion Laboratory California Institute of Technology Pasadena, CA 91103	10. Work Unit No. (TRAIS)
	11. Contract or Grant No. DOT-CG-822868-A
12. Sponsoring Agency Name and Address Commandant (G-DMT-1/TP54) U. S. Coast Guard Headquarters Washington, D.C. 20593	13. Type of Report and Period Covered Final Report.
	14. Sponsoring Agency Code

15. Supplementary Notes

16. Abstract

This report documents the development and subsequent field testing of two rapid response instruments for the detection of methane gas in the vapor resulting from an LNG spill. The instruments were: a laser instrument with a 0.005 second response time and 0.1% sensitivity, and a two-band differential radiometer (TBDR) with a 0.15 second response time and 1% sensitivity. A thermistor sensor was also developed for the rapid (0.2 second) measurement of vapor temperature. The implementation of this instrumentation for Spill Tests LNG-18, LNG-19, LNG-20 and LNG-21 at China Lake, California is also described in this report.

Some comparisons were made between the JPL measurements and those of other organizations involved in the China Lake test program. Good correlation was found, for example, between the laser methane measurement and that of a nearby sensor during LNG-18. During LNG-21 the vapor temperature of methane was also measured and found to be linearly related to the methane concentration over the 2-10% range. In addition to the two methane concentration instruments, progress in the laboratory associated with this program was made on the development of a modified TBDR device to measure the concentration of oxygen in the vapor cloud, and in the development of infrared fiber-optics for advanced laser detection of methane and other species.

17. Key Words	18. Distribution Statement
LNG TBDR LASER METHANE	This document is available to the US public through the National Technical Information Service, Springfield, VA 22161

19. Security Classif. (of this report)	20. Security Classif. (of this page)	21. No. of Pages	22. Price
Unclassified	Unclassified	42	

Form DOT F 1700.7 (8-72) Reproduction of completed page authorized

191 150

INTRODUCTION AND SUMMARY

The Jet Propulsion Laboratory (JPL) was requested by the U. S. Coast Guard to assist in the development of advanced instrumentation for the rapid, sensitive detection of methane gas in the vapor resulting from an LNG spill, and to demonstrate its operation during spill tests at China Lake, California. Two types of instruments were developed: A laser instrument with 0.005 second response time and 0.1% sensitivity, and a two-band differential radiometer (TBDR) with 0.15 second response time and 1% sensitivity. Each of these methane-specific instruments performed real-time measurements at two different locations within the vapor cloud. A thermister sensor was also developed for the rapid (0.2 second) measurement of vapor temperature. Implementation of this instrumentation for Spill Tests LNG-18, LNG-19, and LNG-21 of 8/31/78, 9/13/78, and 11/20/78, respectively, is described in this Report.

Some comparisons have been made between the JPL measurements and those of other organizations involved in the China Lake test program. During LNG-18, good correlation was found between the laser measurement of methane and that of a nearby sensor operated by the Lawrence Livermore Laboratory (LLL). The sensitivity of the laser instrument appears to be several times better than the LLL instrument, and further comparisons should be made using data from LNG-19 and LNG-21. During LNG-21, in addition to methane, the vapor temperature was also measured and found to be linearly related to the methane concentration over the 2-10% range. Quantitatively, the dependence is $-2.13^{\circ}C/\%$ methane, which compares favorably with the theoretical value of $-2.22^{\circ}C/\%$ methane derived by Multhauf of LLL for the conditions of LNG-18.

Laboratory research at JPL associated with this program yielded progress on the development of a modified TBDR instrument to measure the concentration of oxygen in the vapor cloud, and in the development of infrared-transmitting fiber optics for advanced laser detection of methane and other species. Results of the laboratory effort are also described in this Report.

TABLE OF CONTENTS

(cont'd)

TABLE OF CONTENTS (cont'd)

1. Description of JPL Instrumentation

Two different types of instruments were constructed to provide the speed, accuracy, and spatial resolution needed to measure the methane gas concentration during the LNG spill test studies at China Lake, California. One system is based upon the principle of differential absorption of radiation by methane at two narrow wavelength regions in the near infrared (2.1 and 2.3 μm) determined by filters of the broadband radiation from a thermal source. It is called the TBDR, for "two-band differential radiometer," and uses a pathlength of approximately 20 cm. The second instrument is based on the very strong absorption of laser radiation at 3.39 μm by methane, for which a pathlength of only 2 cm is adequate for the test program. During the spill tests, these instruments were situated so as to be engulfed by the vapor cloud as it drifted from the spill point. The TBDR and laser instruments are described in more detail below and in Appendices A and B.

1.1 Two-Band Differential Radiometer (TBDR)

Two identical TBDR instruments were constructed during July and early August. The Block Diagram is illustrated in Figure 1. Calibration was performed on 18 August 1978 using known concentrations of methane gas contained in a 15-cm-long sample cell through which the radiation was transmitted. These concentrations in the cell were 14.7%, 10.0%, and 5.0%, which corresponded to effective concentrations of 11.0%, 7.5%, and 3.75% over the entire 20-cm path. A fourth sample was obtained from the natural gas system supply, and was assumed to be 97% methane, corresponding to 73% over the entire path. Table I lists the absorption measured for each of the TBDR detectors at the sample concentrations indicated:

Table I. TBDR absorption signal for various methane concentrations in a 15-cm-long calibration cell

Methane Concentration (%)	Absorption (%)
14.7	8.
10.0	5.4
5.0	2.8
97.0	40.

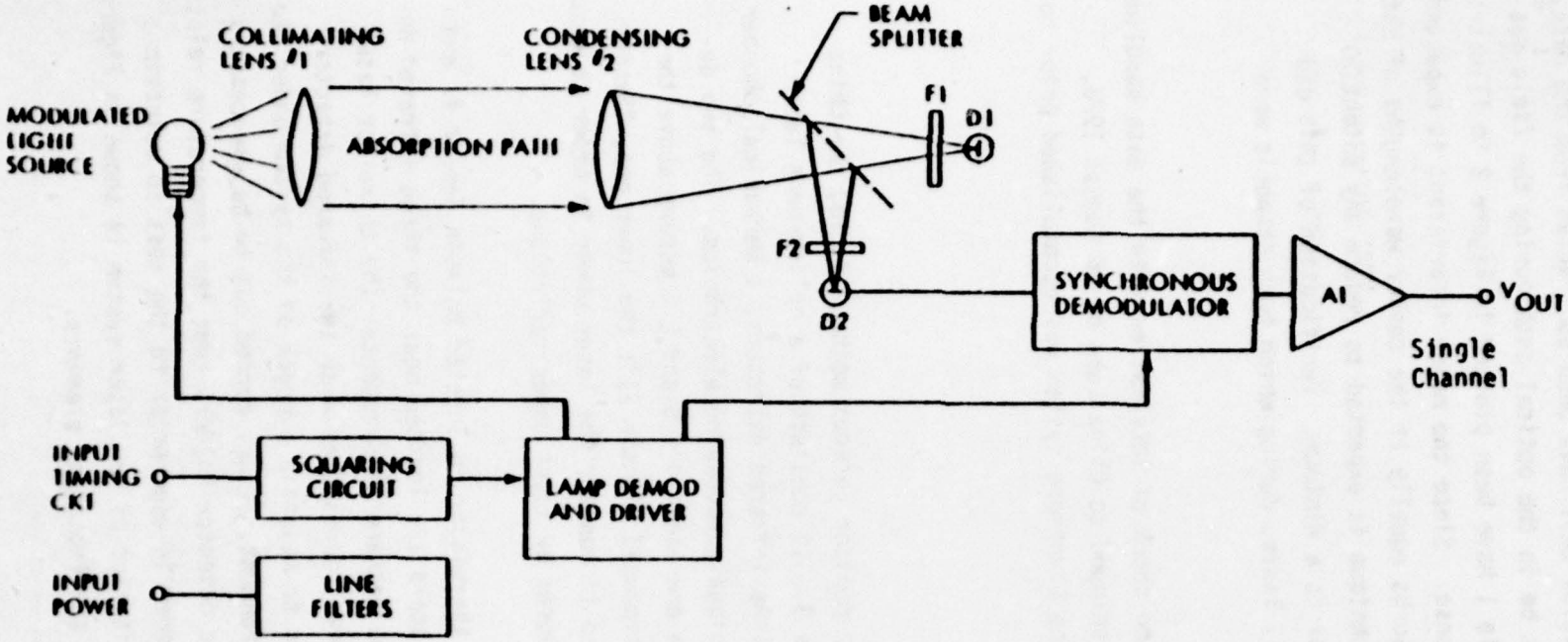

F1, F2: SPECTRAL FILTERS
D1, D2: DETECTORS
A1: AMPLIFIER

Figure 1. Block Diagram for TBDR Sensor Module, showing integration of optics and electronics

Window losses of the calibration cell have been subtracted from the data, since these windows will not be in the optical path during the field measurements. The data of Table 1 have been plotted in Figure 2 to illustrate graphically the system response. Since the major interferant is expected to be water vapor, which absorbs equally at the center wavelengths of each filter, the differential technique is expected to reduce any potential interference from water vapor to a minimum. Verification of this did occur during the actual Spill Tests, during which both channels were monitored.

After the calibration test and check of integration with the data handling system, the TBDR units were shipped to China Lake on 16 August 1978. Checkout and connection to the Livermore system was accomplished prior to the first spill test.

1.2 Laser System

The laser system developed to monitor gaseous methane during the China Lake tests is shown in Figure 3. It consists of a helium-neon laser operating at 3.39 μm, three InAs infrared detectors, a mechanical chopper, and appropriate control and signal-processing electronics. The two detectors for measuring methane are located 1.5 and 2.5 meters above the ground. The upper one is designated "Sensor #1"; the lower one, "Sensor #2." A third detector is used to monitor the laser power in order to ensure that any "signals" are not caused by laser power variations.

An air-temperature measuring thermister is located between Sensor #1 and Sensor #2. Three other thermisters are located near the three infrared detectors (two detectors for the methane measurements; the third for laser power). Thermisters to measure temperatures near the infrared detectors were deemed necessary in order to maintain a check on the system under the rigors of the hot desert environment. (They turned out to be unnecessary because the heat capacity of the detector holders kept the temperature relatively constant.) An air conditioner is used prior to the test to maintain a suitable temperature. The interior of the laser system is shown in Figure 4, which illustrates location of the important elements.

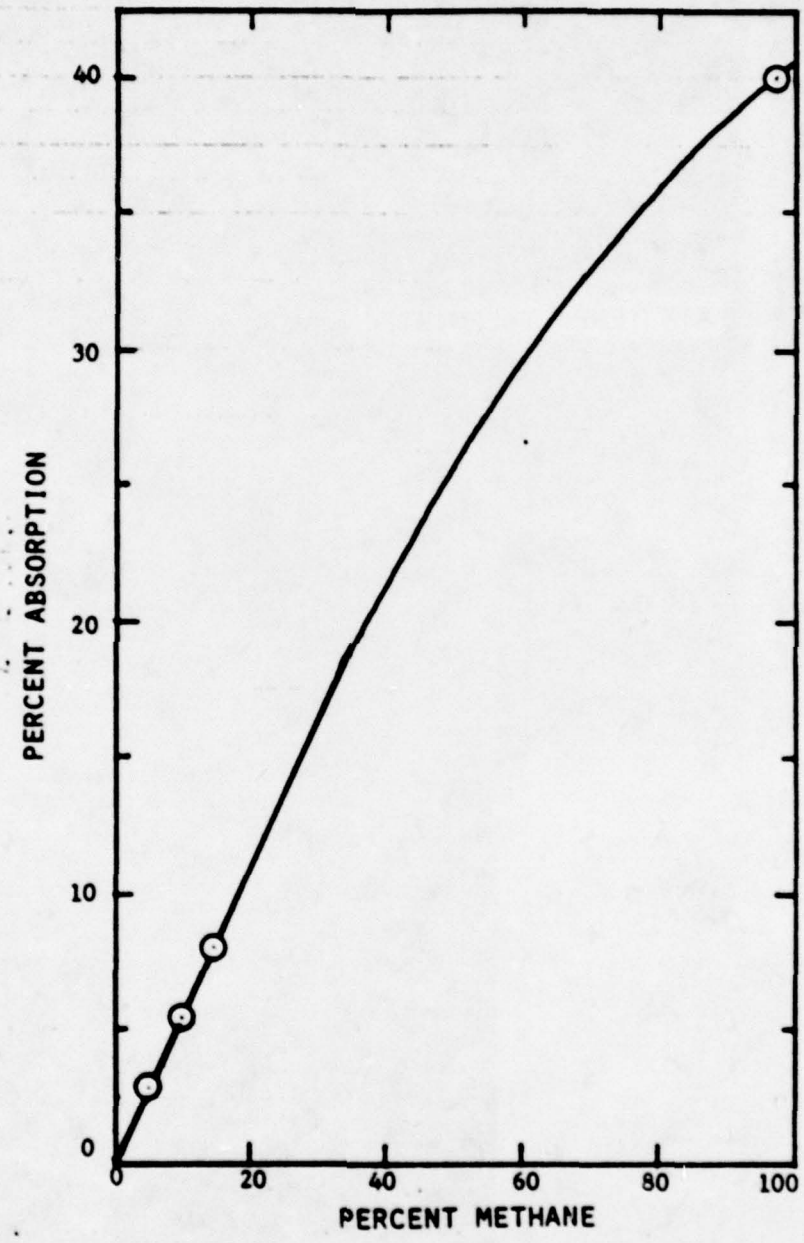

Figure 2. TBDR System response to various methane concentrations

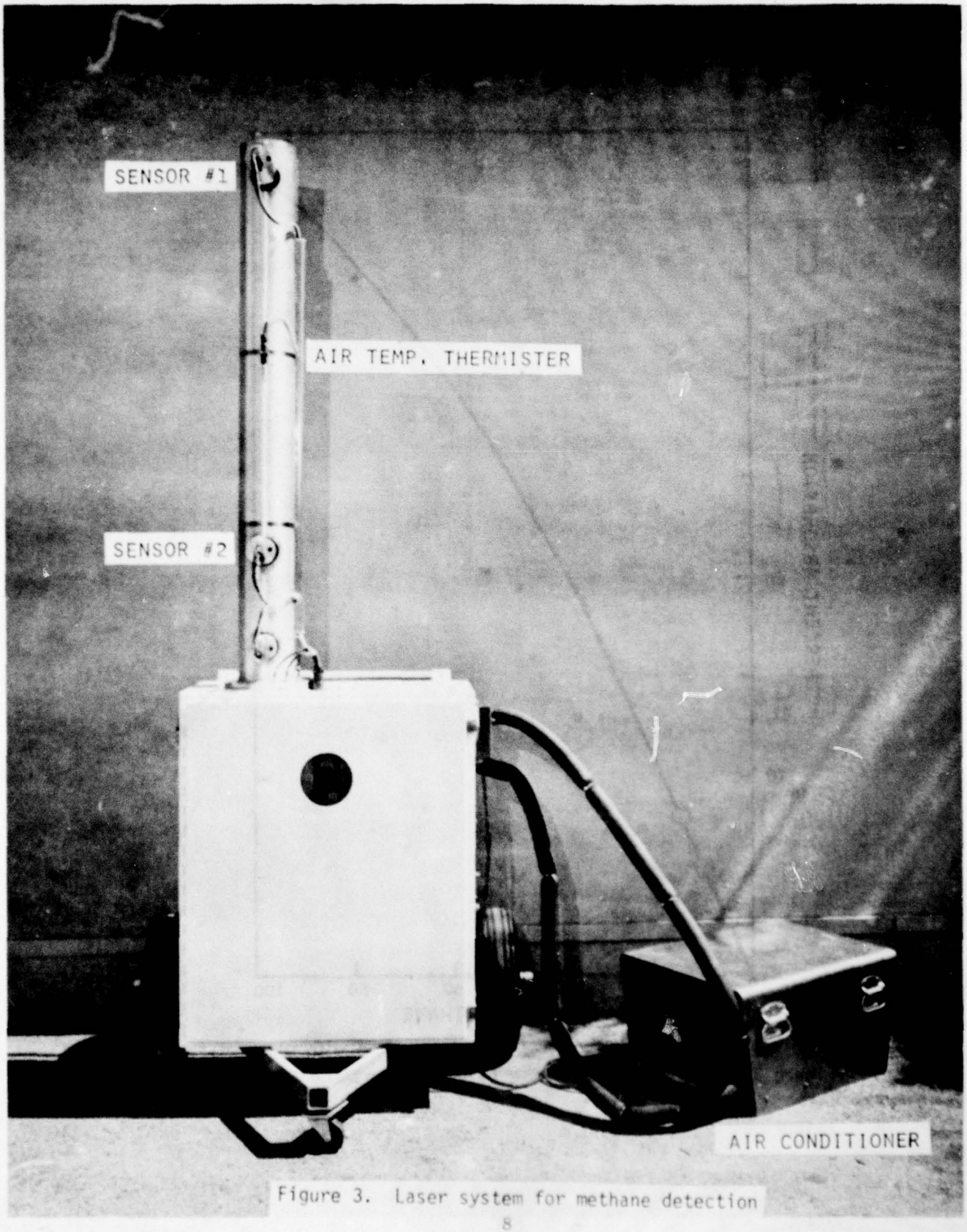

Figure 3. Laser system for methane detection

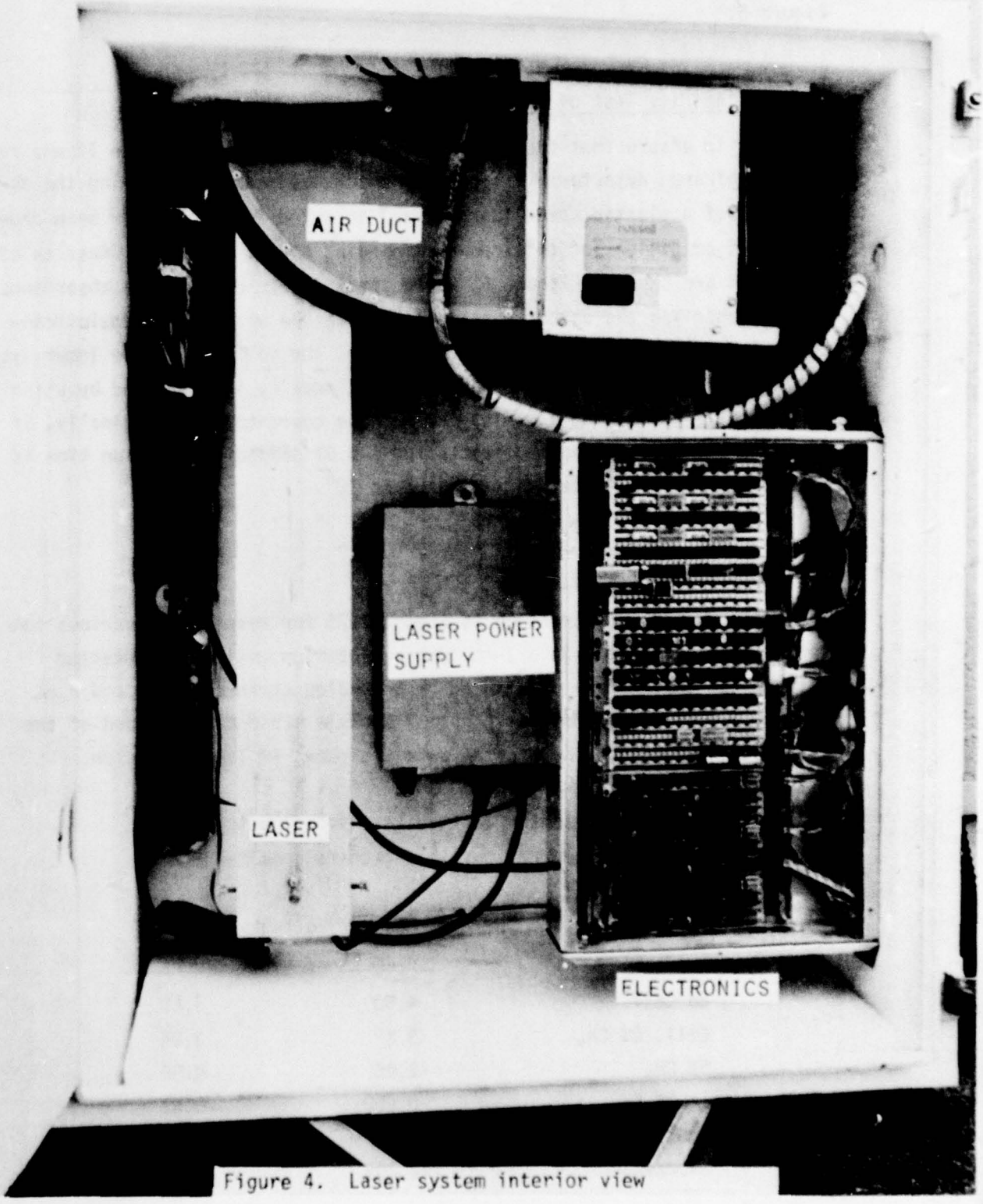

Figure 4. Laser system interior view

The laser instrument has wheels to provide mobility. In addition, it can be oriented vertically; as shown in Figure 3, or horizontally, as illustrated by Figure 5.

1.2.1 Linearity Test of InAs Detectors

In order to ensure that the laser system will operate within the linear range of the infrared detectors, a linearity check was made by observing the absorbance of a plastic sheet (Saran Wrap) inserted into the laser beam under different conditions of total power impinging on the detector. Results of this test are shown in Figure 6, where the ordinate denotes the absorbance and the abscissa the detector voltage. Since the absorbance remains constant to approximately 6 mV on the detector, the voltages of the laser system detectors are kept below this value. Linearity is confirmed by using sample cells containing a variety of methane concentrations. Finally, if the ultimate detector noise limit using a 0.01 second integration time is 6×10^{-9} V, the available dynamic range is 10^6.

1.2.2 Performance Test at JPL

The laser system was tested on 15 August 1978 for response to various concentrations of methane in a 1-cm-long calibration cell. The detector voltage was amplified and measured by an analog strip-chart recorder as well as a digital voltmeter. Figure 7 shows a strip-chart record of the calibration signals. The digital data are shown in Table II below.

Table II. Amplified detector voltage corresponding to various methane concentrations in a 1-cm-long cell.

	Sensor Voltages (V)	
Absorber	Sensor #1	Sensor #2
No Cell	4.50	3.85
Cell, 0% CH_4	3.47	3.05
5% CH_4	1.46	0.98
14.7% CH_4	-0.660	-0.83
100% CH_4	-2.497	-2.498
Blocked	-2.499	-2.500

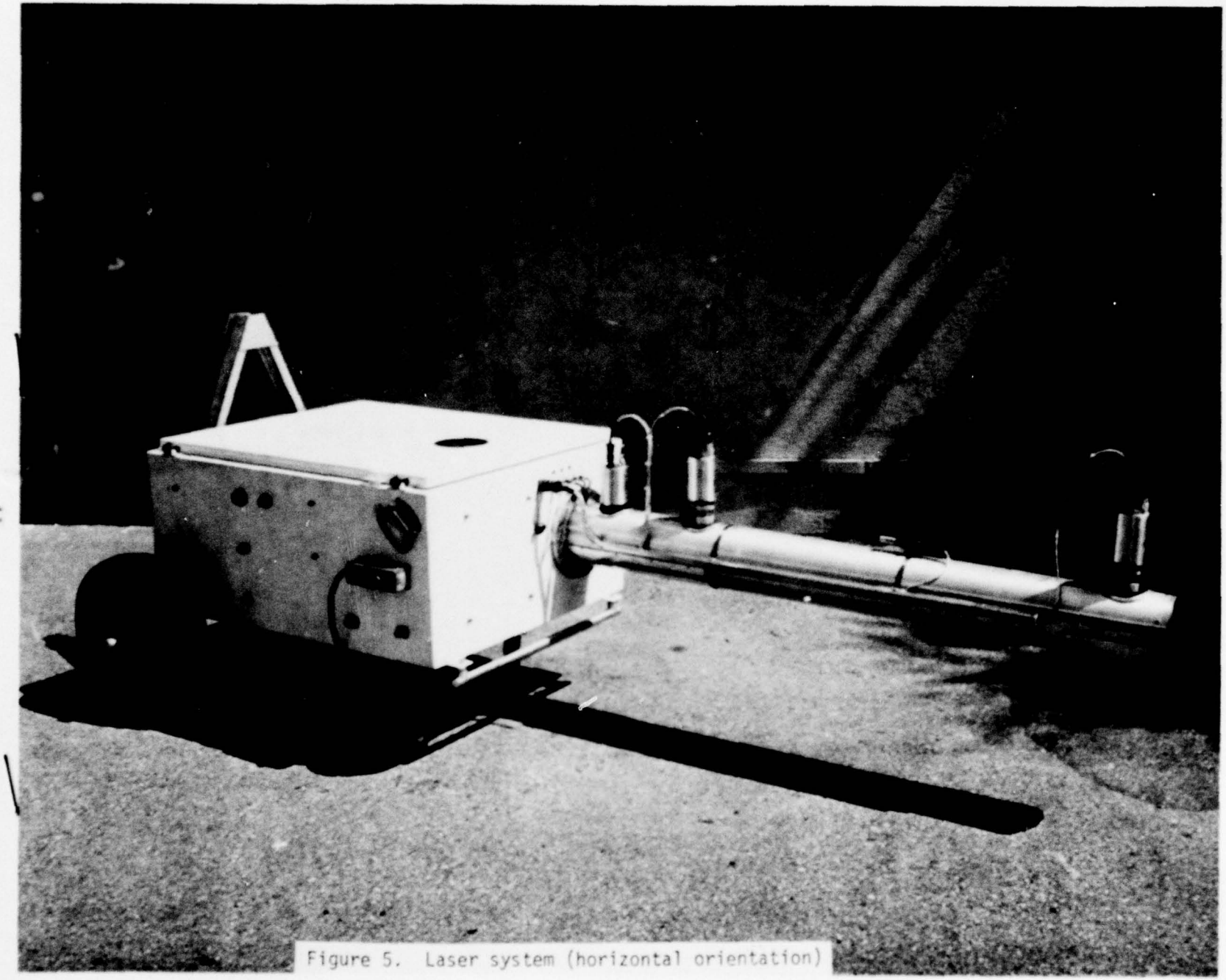

Figure 5. Laser system (horizontal orientation)

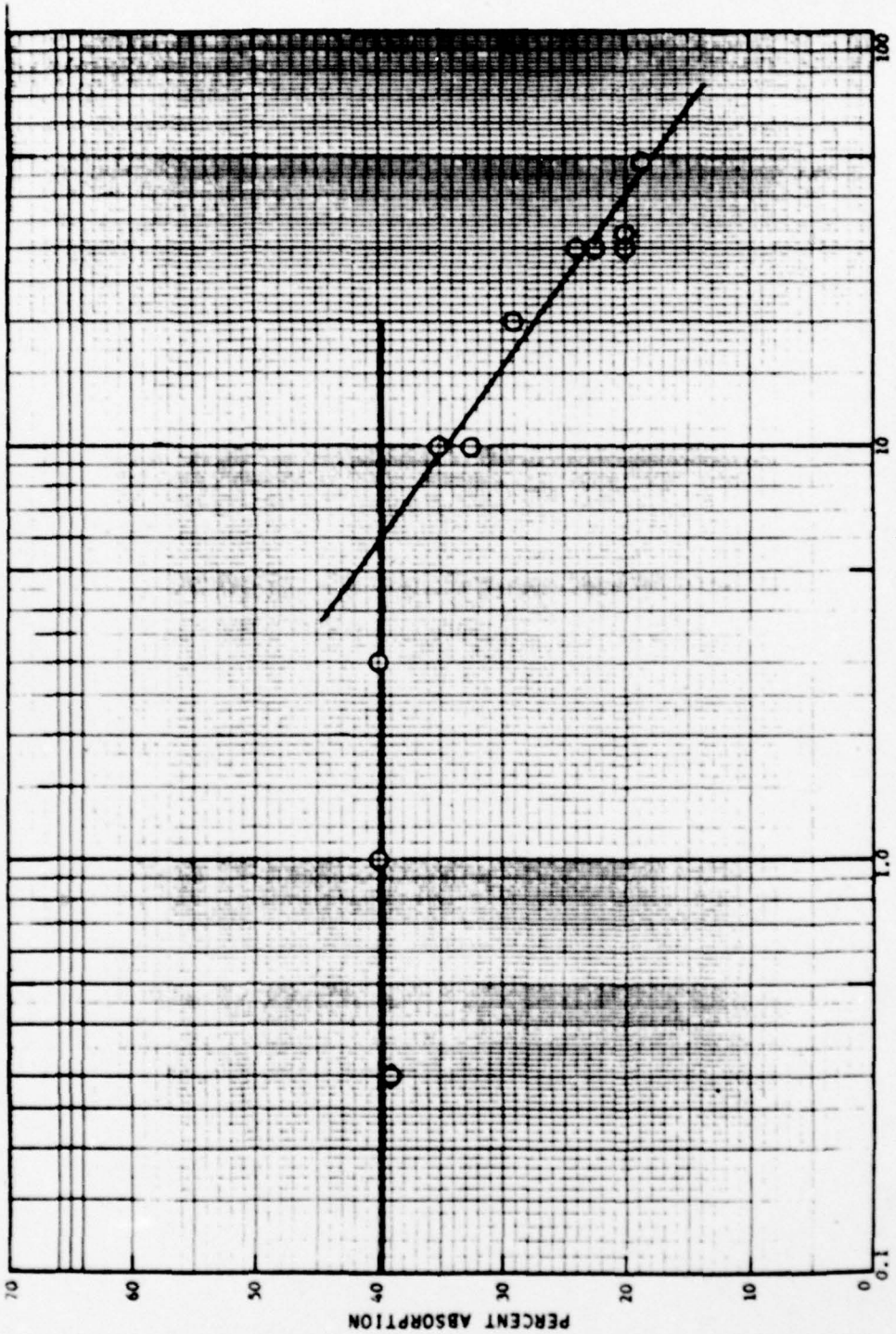

Figure 6. Linearity test of InAs detector at 3.39 μm wavelength

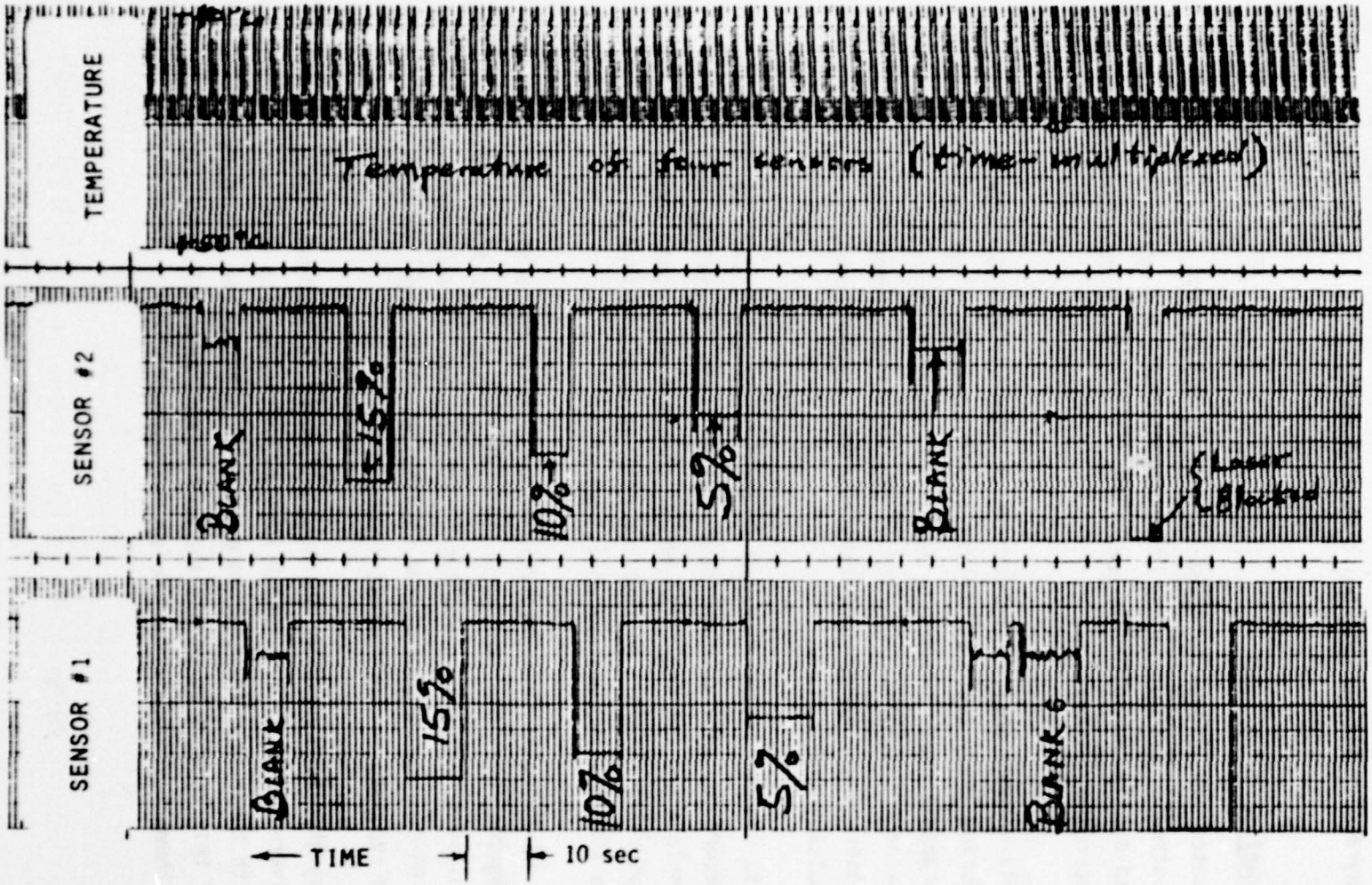

Figure 7. Calibration test of laser system for methane detection

These results are plotted in Figure 8 in order to demonstrate system linearity and agreement between the two sensor channels.

1.2.3. Shipment to China Lake

The laser system was shipped to China Lake on 18 August 1978. Integration with the electronics systems in the Livermore trailer, and system checkout, were performed during the following week. The laser system incorporates four data recording systems:

1) Six-channel analog recorder (which operates at 2.5 cm/sec during spill test) at the spill test location. The six channels are: Sensor #1; amplified Sensor #1 for high methane concentrations; Sensor #2; amplified Sensor #2; laser power; system temperatures (four temperatures, multiplexed).

2) Six-channel analog recorder at the Livermore trailer, to record the same data as above, but with the capability to replace the two amplified sensor channels with logarithmic-converted channels so that the methane concentration will be linear with recorder divisions.

3) A JPL magnetic tape recorder, which records the above data, together with the TBDR data and time information, after the voltages have been converted to frequencies via voltage-to-frequency converters at the spill site. This tape can then be replayed in any desired format.

4) Magnetic tape recorder operated and owned by Lawrence Livermore Laboratory, which records the above data together with those from the Livermore and USCG instruments. Purpose of this tape is to permit the development and evaluation of mathematical models for the vapor clouds.

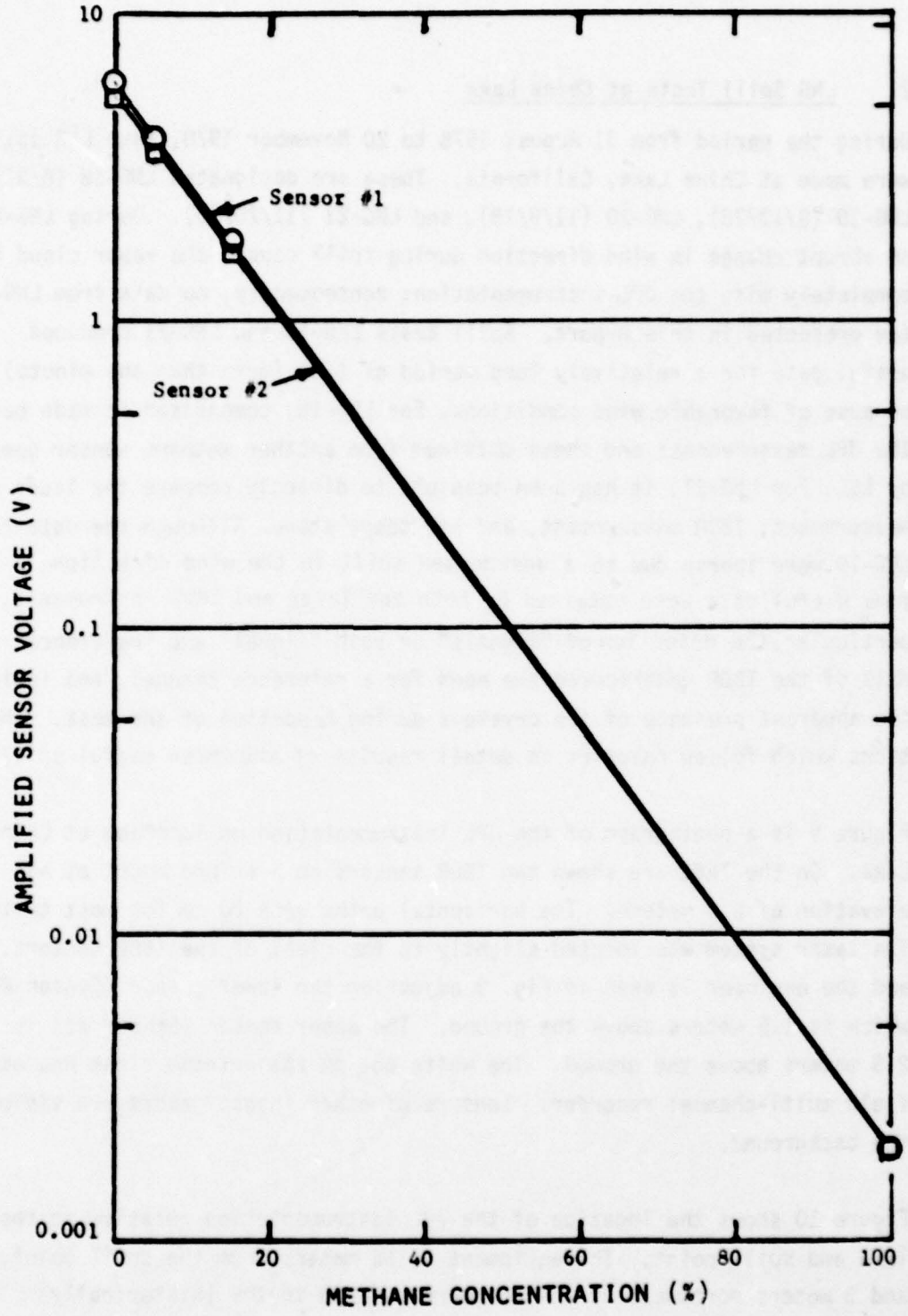

Figure 8. Response of laser system sensors to various methane concentrations in a 1.0-cm calibration cell (digital voltmeter measurements)

2. LNG Spill Tests at China Lake

During the period from 31 August 1978 to 20 November 1978, four LNG spills were made at China Lake, California. These are designated LNG-18 (8/31/78), LNG-19 (9/13/78), LNG-20 (11/9/78), and LNG-21 (11/20/78). During LNG-20 an abrupt change in wind direction during spill caused the vapor cloud to completely miss the JPL instrumentation; consequently, no data from LNG-20 are presented in this Report. Spill tests LNG-18 and LNG-21 produced useful data for a relatively long period of time (more than one minute) because of favorable wind conditions. For LNG-18, comparison is made between the JPL measurements and those obtained from another methane sensor operated by LLL. For LNG-21, it has been possible to directly compare the laser sensor measurement, TBDR measurement, and air temperature. Although the data for LNG-19 were sparse due to a unexpected shift in the wind direction, some useful data were obtained by both the laser and TBDR instruments. In particular, the detection of "signals" on both "signal" and "reference" channels of the TBDR underscored the need for a reference channel, and indicated the apparent presence of ice crystals during a portion of the test. The subsections which follow describe in detail results of the three useful spill tests.

Figure 9 is a photograph of the JPL instrumentation on location at China Lake. On the left are shown two TBDR sensors on a tripod mount at an elevation of 0.5 meters. The horizontal paths were 20 cm for most tests. The laser system was located slightly to the right of the TBDR sensors, and the engineer is seen in Fig. 9 adjusting the lower sensor (Sensor #2) which is 1.5 meters above the ground. The upper sensor (Sensor #1) is 2.5 meters above the ground. The white box on the extreme right houses the field multi-channel recorder. Sensors of other investigators are visible in the background.

Figure 10 shows the location of the JPL instrumentation relative to the lake and spill point. The equipment is 55 meters from the spill point, and 3 meters northwest of a line corresponding to the (historically) average wind direction (see Fig. 11).

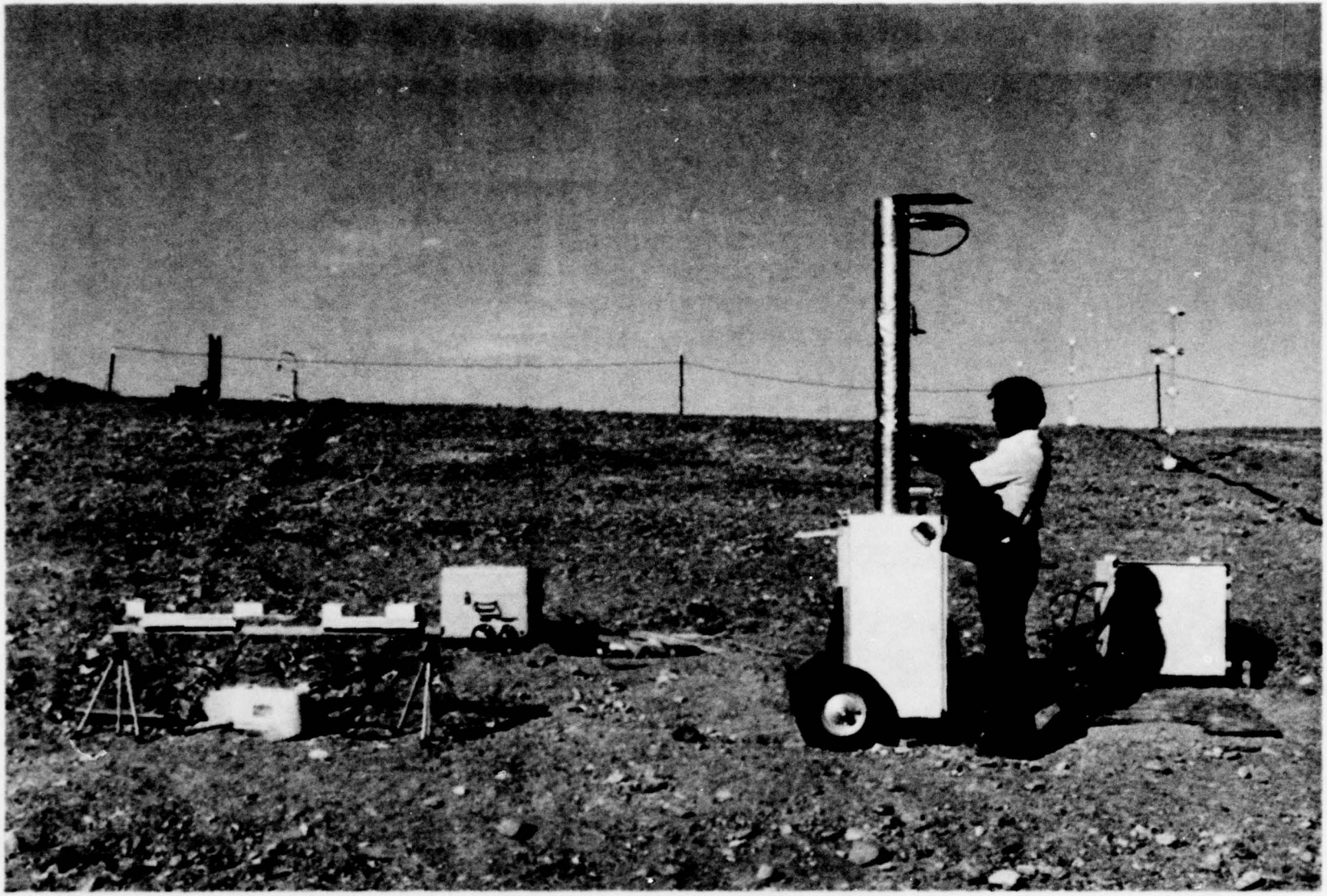

Figure 9. Photograph of JPL instrumentation at China Lake

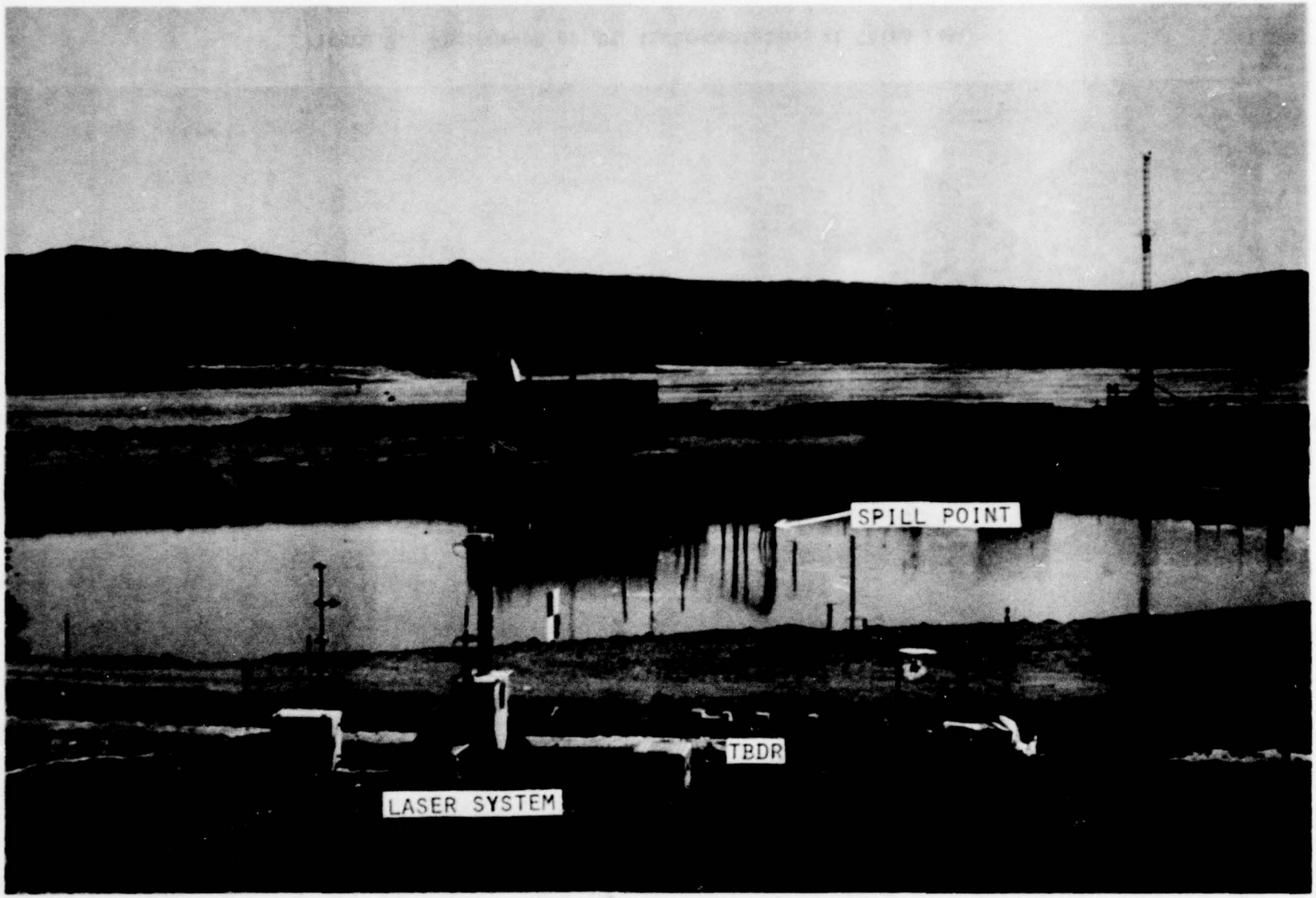

Figure 10. Photograph showing location of JPL instrumentation relative to spill point.

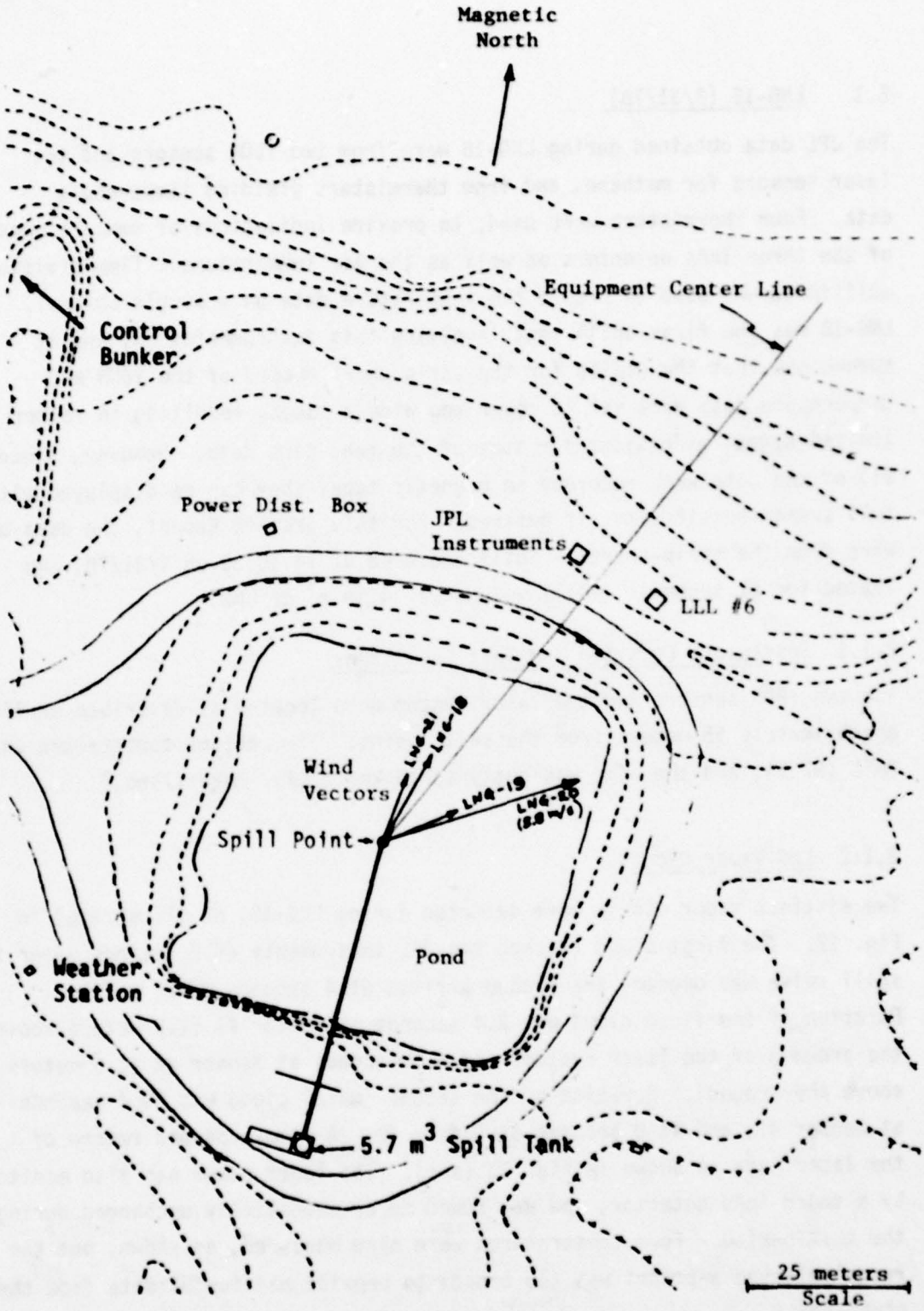

Figure 11. Contour plot of LNG Spill Test Site, indicating location of JPL instrumentation and LLL Site #6. Also shown are the average wind vectors for each of the four spill tests (from R. Koopman).

2.1 LNG-18 (8/31/78)

The JPL data obtained during LNG-18 were from two TBDR sensors and two laser sensors for methane, and from thermisters yielding temperature data. Four thermisters were used, to provide indications of temperatures of the three InAs detectors as well as the air temperature. Time-division mulitiplex was used to record the temperature data on a single channel. LNG-18 was the first spill test involving this instrumentation, and it turned out that the scales for the strip-chart record of the TBDR and temperature data were set to cover too wide a range, resulting in rather limited signal excursions for some of the real-time data. However, since all of the data were recorded on magnetic tape, they can be displayed with full system sensitivity, if desired. For this present Report, the data used were from the strip-charts. Spill occurred at 14:56:30 on 8/31/78, and lasted for 67 seconds. Spill volume was 4.39 m^3 of LNG.

2.1.1 Instrument Location and Test Conditions

The two TBDR sensors and the laser system were located as described earlier, approximately 55 meters from the spill point. The ambient temperature was 36°C (97°F), and the wind was gusty to 15 knots (7.7 meters/sec.).

2.1.2 LNG Vapor Clouds

Two distinct vapor clouds were detected during LNG-18, as illustrated in Fig. 12. The first cloud reached the JPL instruments 40.2 seconds after the spill valve was opened; the second arrived 61.4 seconds after spill. Duration of the first cloud was 2.4 seconds at Sensor #1 (2.5 meters above the ground) of the laser system, and 4.6 seconds at Sensor #2 (1.5 meters above the ground). Duration of the second (main) cloud was 39.4 seconds at Sensor #1, and 41.0 seconds at Sensor #2. A time-expanded record of the laser data is shown in Fig. 13 (a-c). The laser power was also monitored by a third InAs detector, and was found to be essentially unchanged during the test period. Four temperatures were also measured, as shown, but the range selected a-priori was too broad to provide meaningful data from the strip-chart.

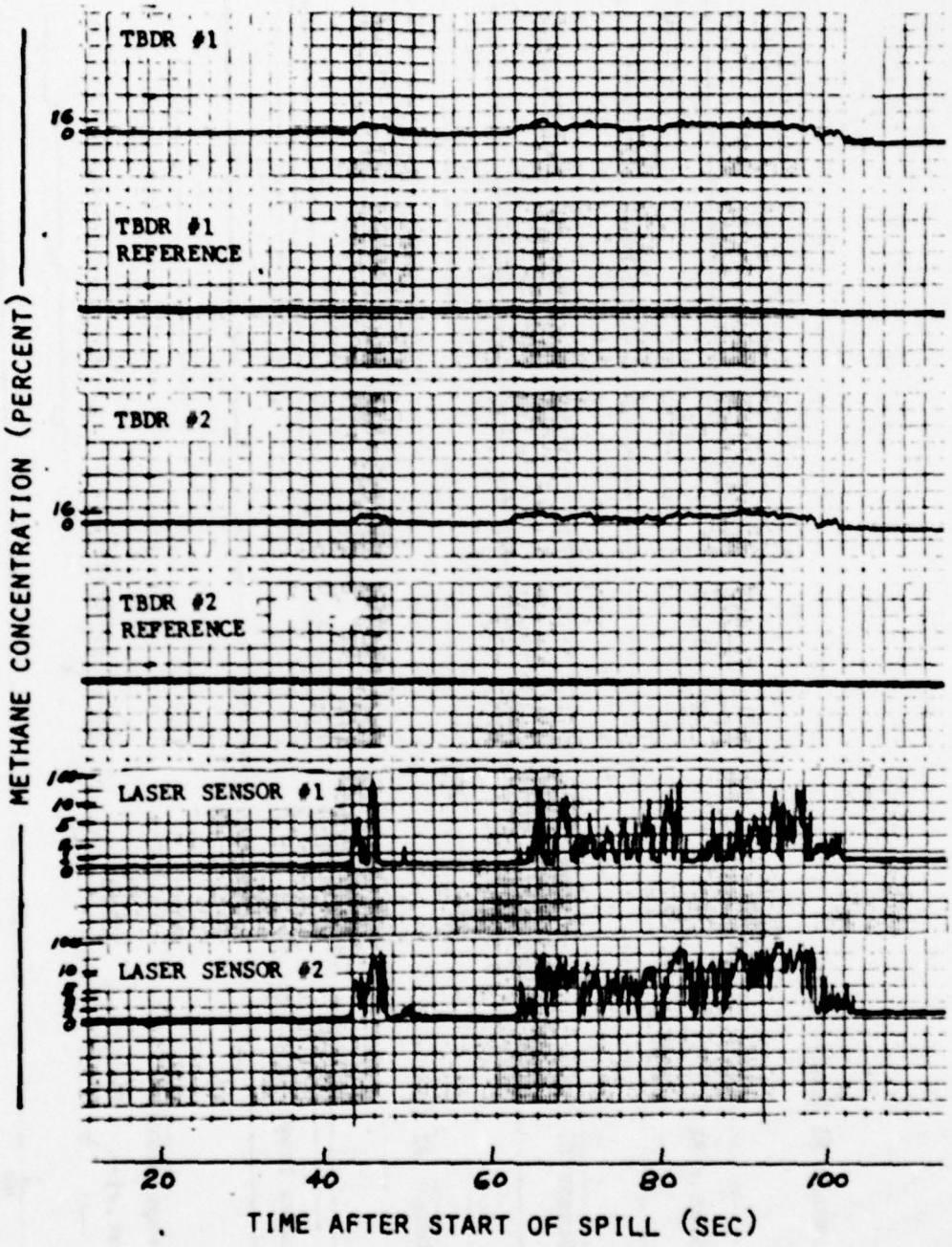

Figure 12. JPL sensor measurements of methane during LNG-18 Spill Test

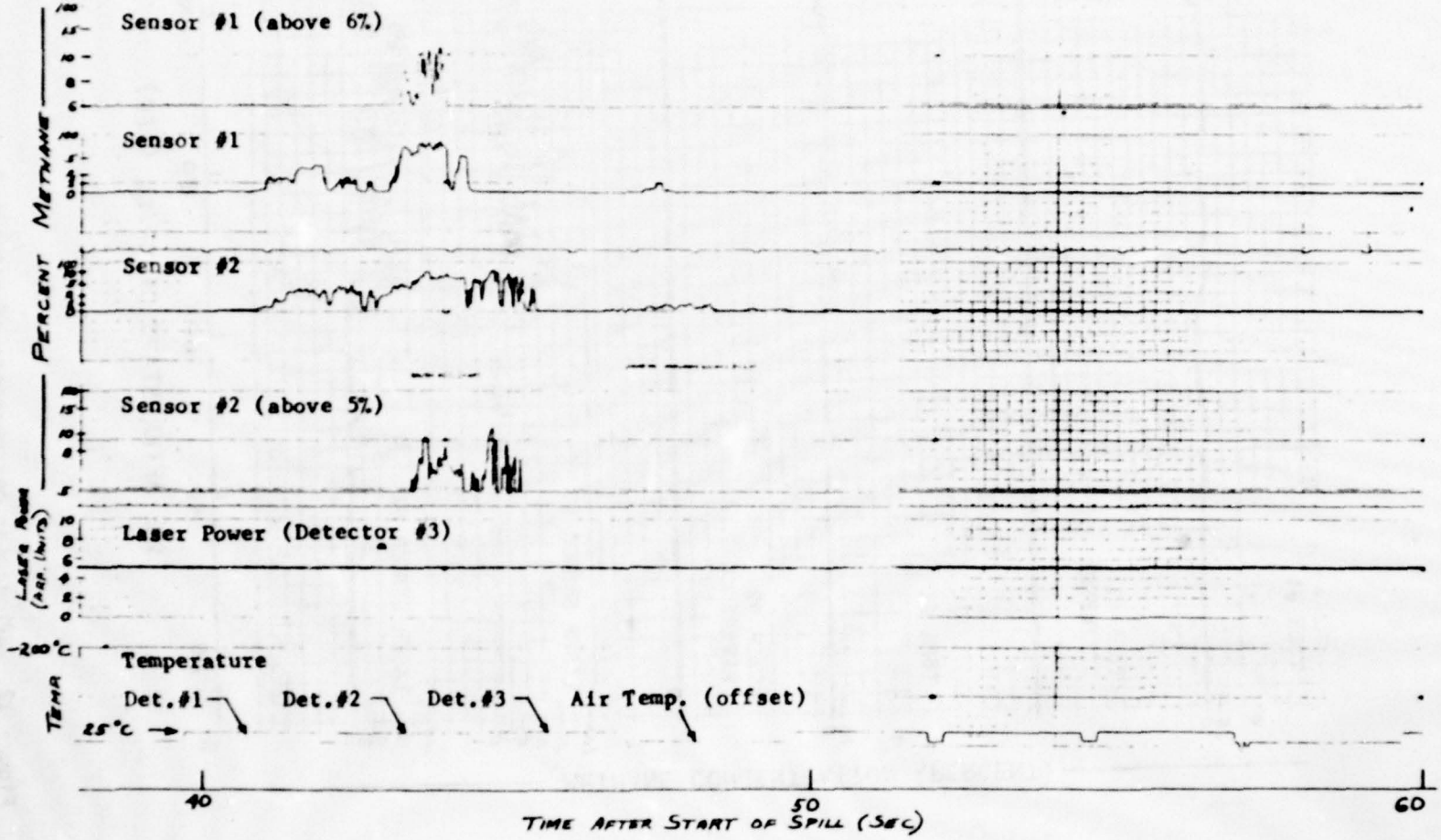

Figure 13 (a). LNG-18 Spill Test: Time-expanded measurements of methane concentration, laser power, and temperature

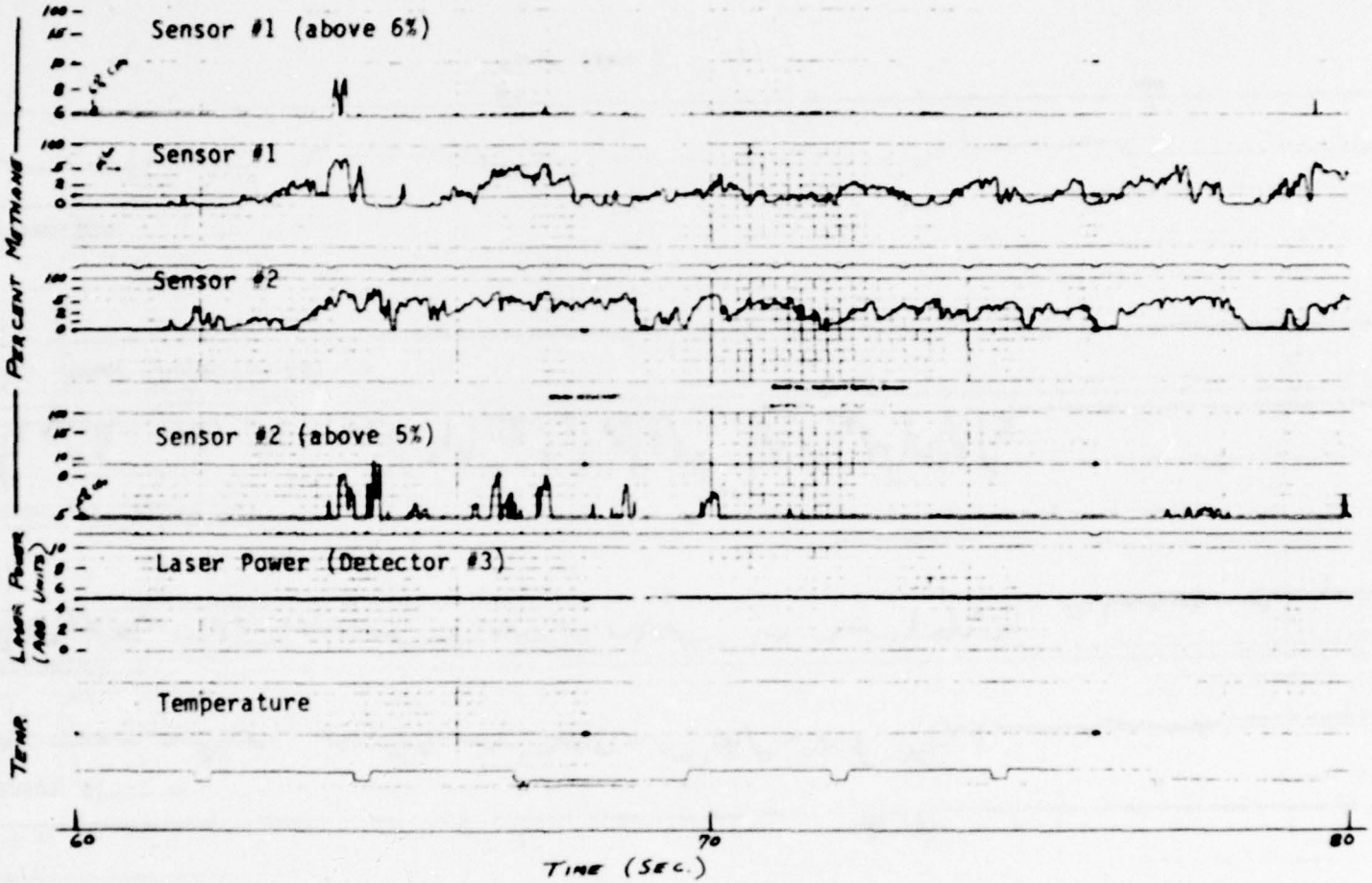

Figure 13 (b). LNG-18 Spill Test: Time-expanded measurements of methane concentration, laser power, and temperature (cont'd)

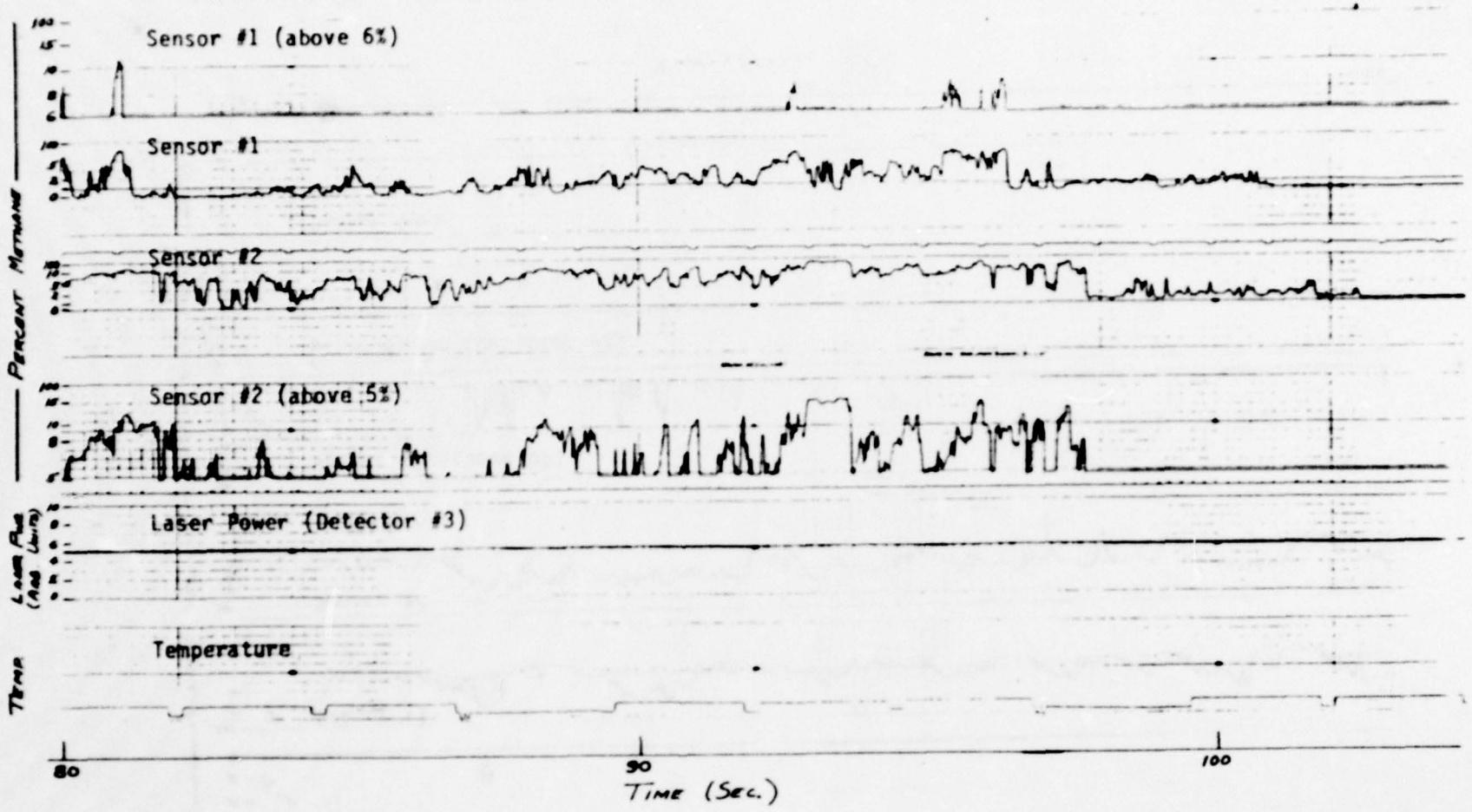

Figure 13 (c). LNG-18 Spill Test: Time-expanded measurements of methane concentration, laser power, and temperature (cont'd)

The maximum methane concentration in the first cloud was 11.1% at Sensor #1, and 10.9% at Sensor #2. These occurred at times of 43.6 sec and 44.7 sec, respectively. The maximum methane concentration in the second cloud was 11.4% at Sensor #1, and 14.2% at Sensor #2. These occurred at times of 80.8 seconds and 93.4 seconds, respectively, after the spill valve was opened. As expected, these values are somewhat lower than those measured by the TBDR instrument, which is located closer to the ground where the cooler, heavier gas is expected to be. The TBDR data did not exhibit the expected rapid time of response (0.15 seconds); presumably, this is due to path-averaging over the 20-cm optical path, which is not as pronounced in the 2-cm path of the laser system.

2.1.3 Time Above 5% Methane

Since methane gas can be explosive in the 5-15% concentration range, it may be useful to know the extent of time the 5% value was exceeded in both of the observed vapor clouds:

First Cloud: Sensor #1 (h = 2.5 meters) showed that the methane concentration was above 5% for 0.89 ± 0.01 seconds, or 26% of the duration of the first cloud. Sensor #2 (h = 1.5 meters) showed that the 5% value was exceeded for 1.40 ± 0.01 seconds, or 30% of the total time the cloud was present.

Second (Main) Cloud: Sensor #1 indicated that the 5% value was exceeded for 2.5 ± 0.1 seconds, or 6.3% of the second cloud's duration, whereas Sensor #2 yielded corresponding values of 14.5 ± 0.1 seconds and 35%.

2.1.4 Discussion of LNG-18

In addition to providing numerical data on the vapor clouds of LNG-18, a comparison was made between the methane measurements of Sensor #2 and the TSI data recorded at 1-m elevation by LLL at Station 6, located 24 meters away, but the same distance from the spill point (see Figure 11). Figure 14 illustrates a surprisingly good correlation between the TSI and laser measurements in concentration and time. This suggests that both instruments are working well and are calibrated properly.

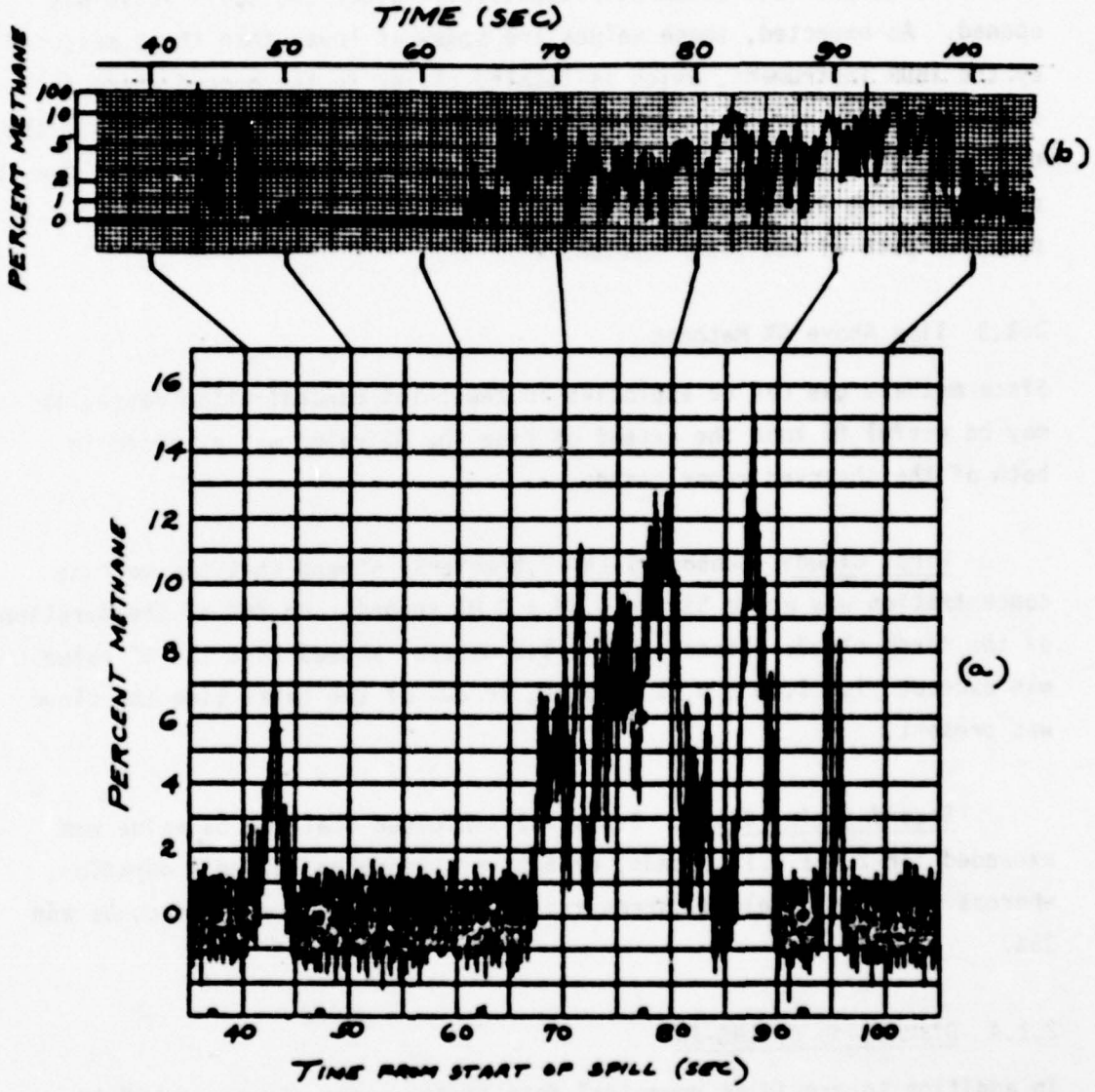

Figure 14. Methane concentration measurements for LNG-18 Spill Test obtained from (a) Lawrence Livermore Laboratory TSI sensor at Station 6 (From R. Koopman, Memorandum of 10/30/78, Fig. 9) and (b) from JPL Laser Sensor #2.

2.2 LNG-19 (9/13/78)

In order to accommodate a Raman lidar system for one spill test, LNG-19 was performed in the darkness of early evening, at 7:30 p.m. The spill lasted for 63 seconds, with both TBDR units and both laser sensors operational.

2.2.1 Instrument Location and Test Conditions

The instrument locations for LNG-19 were the same as for LNG-18, approximately 55 meters from the spill point. At the time of the spill, the wind direction shifted from SW to WSW, with the result that most of the vapor cloud missed the JPL instrumentation. Useful data were obtained, however, and are presented below. Wind speed was 15-20 knots.

2.2.2 LNG Vapor Clouds

Figure 15 illustrates the methane concentration data obtained by one of the TBDR units (the other did not exhibit any signal change) and the two laser sensors. Several small puffs were observed. The first puff occurred at 40.4 seconds after start of spill, lasted for 1.0 second at Laser Sensor #1, and 1.5 seconds at Laser Sensor #2. Peak concentrations were 0.28% and 1.28%, respectively.

The second puff occurred at 95.0 seconds at Sensor #1, and 93.2 seconds at Sensor #2, lasting for 1.0 second and 3.8 seconds, respectively, with peak concentrations of 0.44% and 1.46%.

The third puff occurred at 105.2 seconds at Sensor #1, lasting for 0.28 seconds. That same puff lasted for 0.12 seconds at Sensor #2. The peak concentrations were 0.14% and 0.12% for Sensors #1 and #2, respectively.

2.2.3 Discussion of LNG-19

Although the bulk of the vapor from Spill Test LNG-19 missed the JPL instrumentation, several small puffs of methane-laden vapor were detected and quantified. The maximum recorded concentration was 1.28% methane. Figure 15 shows interference in the reference channel of the TBDR unit, suggesting the presence of ice crystals in the beam, and demonstrating the need for such a reference channel in this instrument.

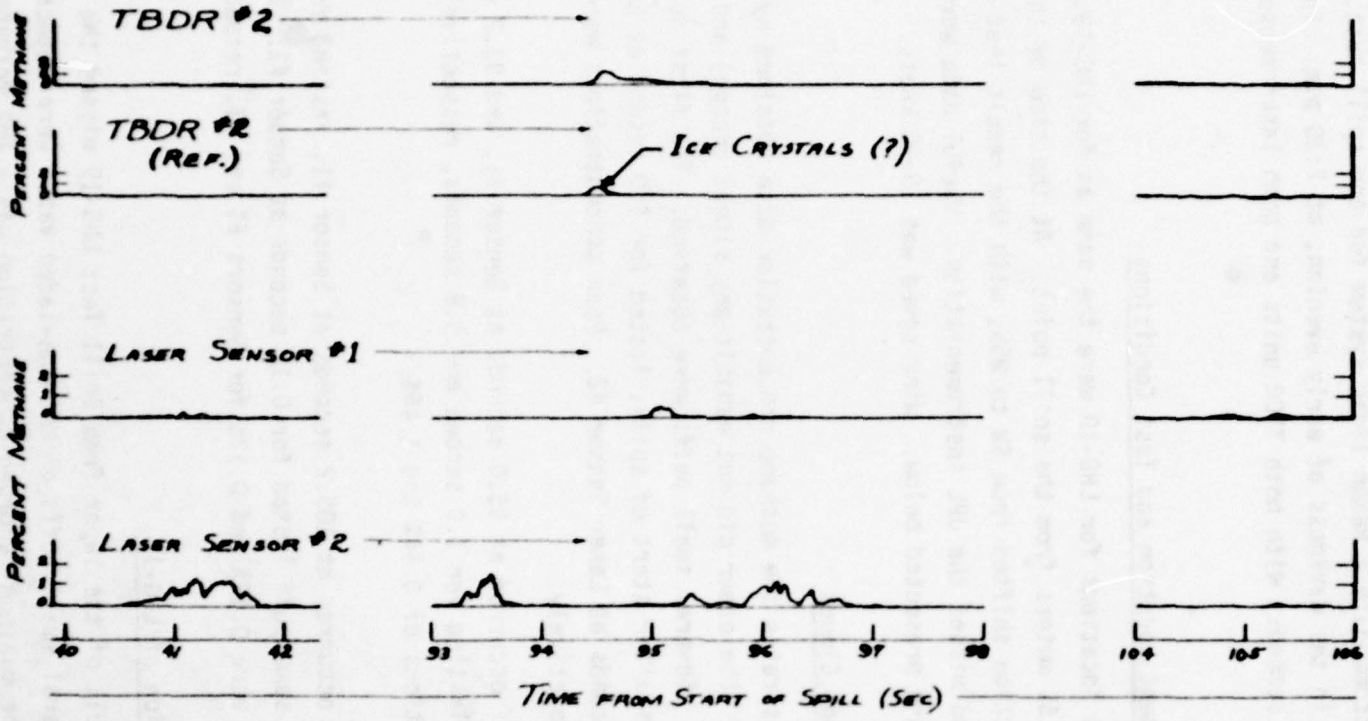

Figure 15. Methane concentration measurements for LNG-19 Spill Test

2.3 LNG-21 (11/20/78)

For this spill test, the last in the current series, both laser sensors, one TBDR sensor, and the thermister for measuring air temperature were operational. (The other TBDR unit had been returned to the laboratory for further studies.) Spill occurred at 3:10 p.m, and lasted for approximately 58 seconds.

2.3.1 Instrument Location and Test Conditions

The location of the JPL instruments remained the same as for the earlier tests, but only one TBDR unit was used, and it was situated very near (within 20 cm) the Laser Sensor #2 in order to obtain correlative measurements. The air-temperature-measuring thermister was moved down the laser instrument column to within a few cm of Sensor #2 also, and the time-division multiplex circuit was modified so that a continuous measurement of air temperature could be recorded during the test. Laser Sensor #1 provided data 2.5 meters above the ground, as before.

The wind direction before the spill was from the SW, averaging 5-10 knots. At time zero it shifted toward the SSW, and one minute later back toward the SW. The effect of this on the JPL measurements was that no indication of methane was observed until nearly one minute after spill, at which time the change in wind direction brought the main cloud in the vicinity of the instruments.

2.3.2 LNG Vapor Clouds

The JPL instruments recorded over 70 seconds of continuous data. Figure 16 (a-b) shows the laser data, illustrating two puffs of methane-laden vapor. The first puff occurred at 57.2 seconds after spill, and lasted for 0.3 seconds at Sensor #1 and 1.5 seconds at Sensor #2. Peak concentrations were 1.8% and 3.8% at 58.0 and 58.2 sec, respectively. The main cloud occurred at 64.2 seconds, and lasted for 61.7 seconds at Sensor #1, and 63.2 seconds at Sensor #2. Peak concentrations were 11.9% and 13.5% at 73.0 and 73.3 sec, respectively, at the two sensor locations.

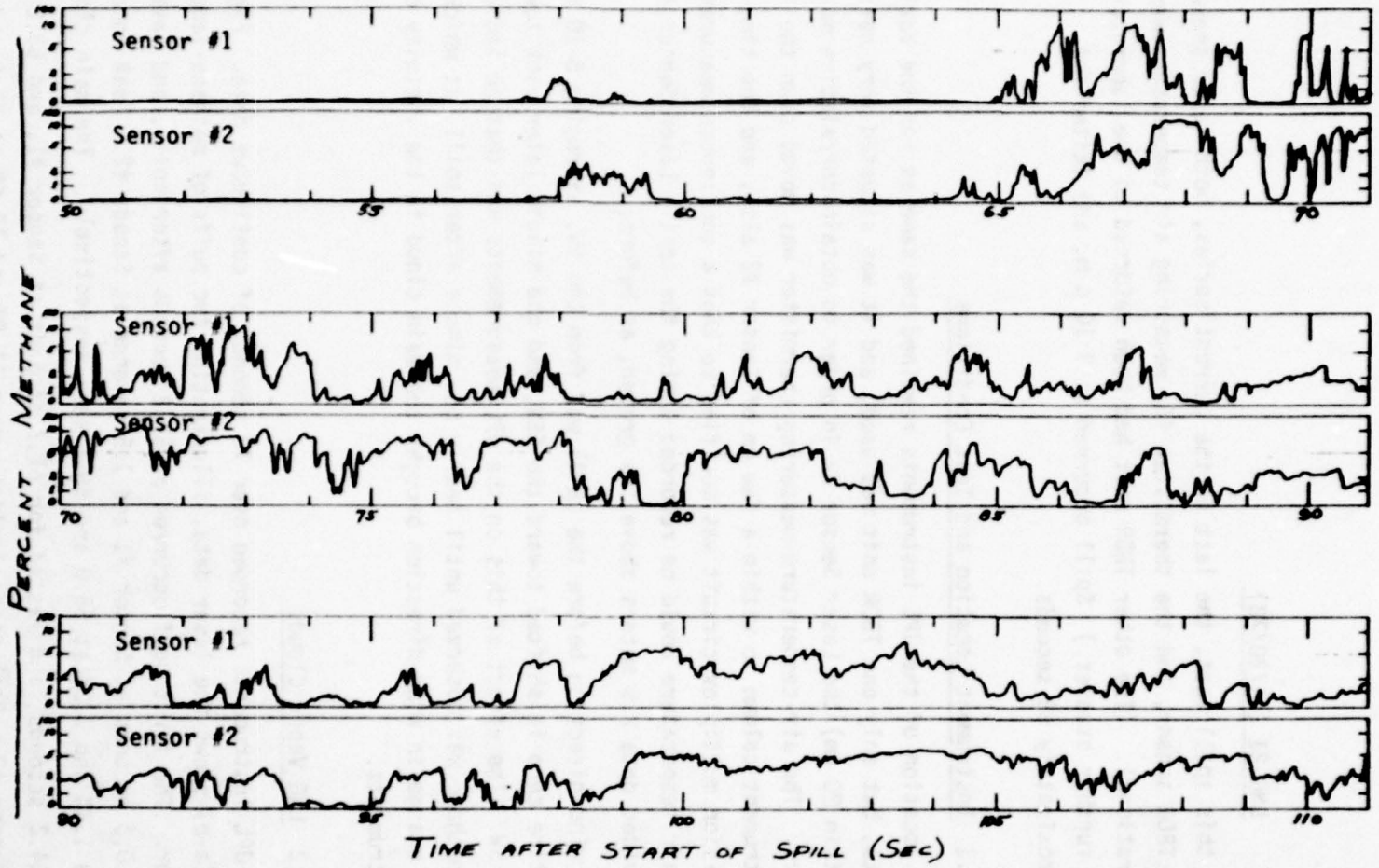

Figure 16(a). Laser sensor measurements of methane concentration for LNG-21 Spill Test

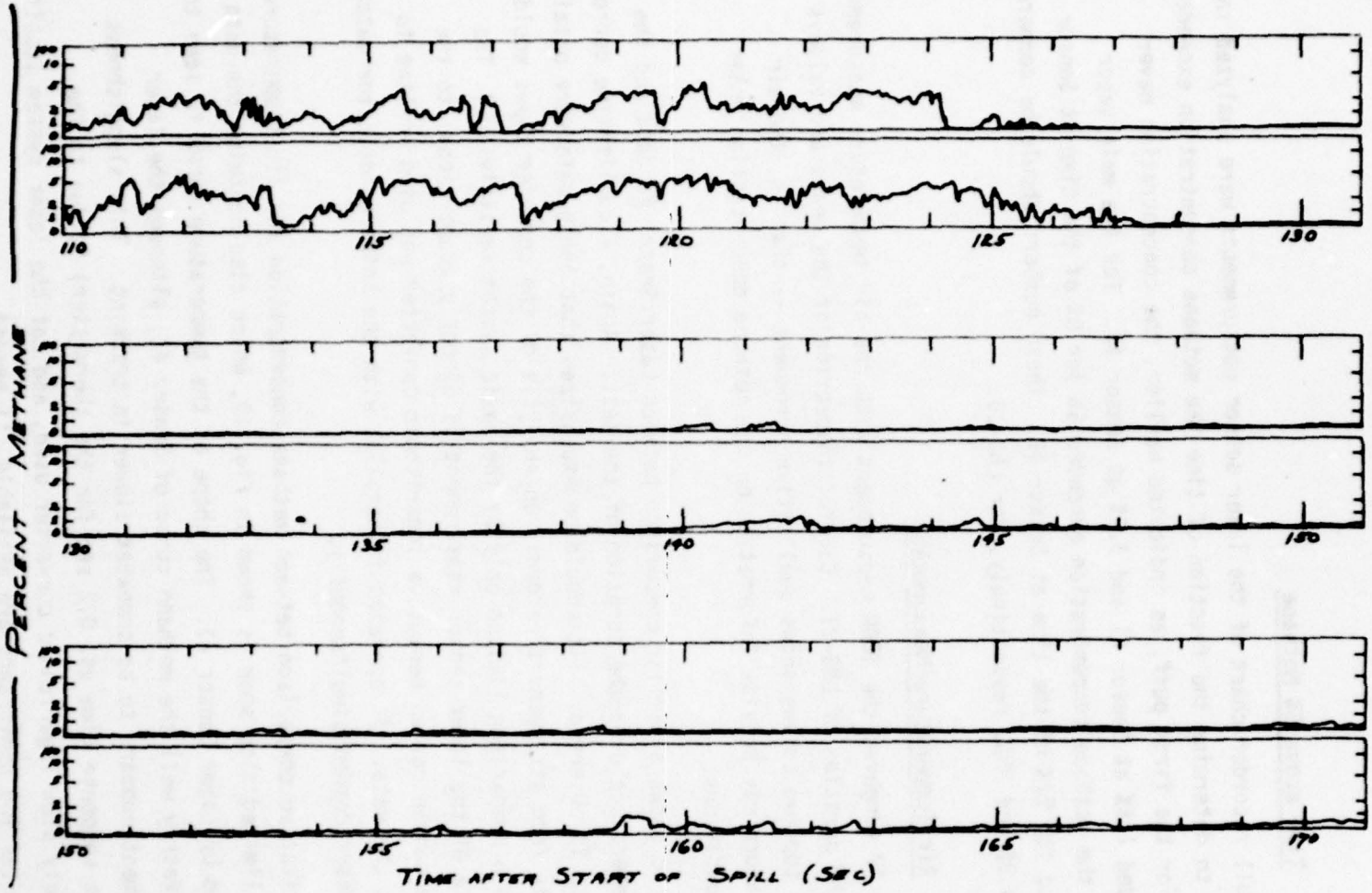

Figure 16(b). Laser sensor measurements of methane concentration for LNG-21 Spill Test (cont'd)

2.3.3 Time above 5% Methane

The full recorder chart of the laser sensor measurements were analyzed in order to determine the fraction of time the methane concentration exceeded 5%. For the first puff, as indicated earlier, the concentration never exceeded 1.8% at Sensor #1 and 3.8% at Sensor #2. For the main vapor cloud the methane concentration exceeded 5% for 8% of the time at Sensor #1, and for 27% of the time at Sensor #2. These numbers should be compared with 6.3% and 35%, respectively, for LNG-18.

2.3.4 Air Temperature Measurement

Figure 17 compares the TBDR measurement with the air temperature measurement over the duration of LNG-21. Careful inspection of the peaks and valleys of the top two curves shows qualitative agreement -- that is, the air temperature may provide information on the methane concentration under some conditions.

Figure 18 shows a similar comparison between Laser Sensor #2 data and the air temperature over the duration of the test. Again, a qualitative correspondence is observed. (It should be emphasized that these data were obtained directly from strip-chart records; an analysis of the computer tapes would provide a comparison limited only by the basic system sensitivity.) The ordinate of the laser sensor measurement is directly proportional to the methane concentration because a logarithmic converter was used on-line to convert the data. It operated in parallel with the infrared detector output, which was recorded simultaneously.

A quantitative comparison between methane concentration and air temperature over a limited time span is shown in Fig. 19, which also contains the data recorded by Laser Sensor #1. The shape of the temperature curve is seen to follow fairly well the methane curve of Sensor #2, although the laser measurement appears to be somewhat slower in tracking. This sluggishness (0.4 sec response time vs. 0.2 sec for the thermister) is due to the relatively slow logarithmic converter used, and not the laser system itself. Much faster log converters are available, if needed.

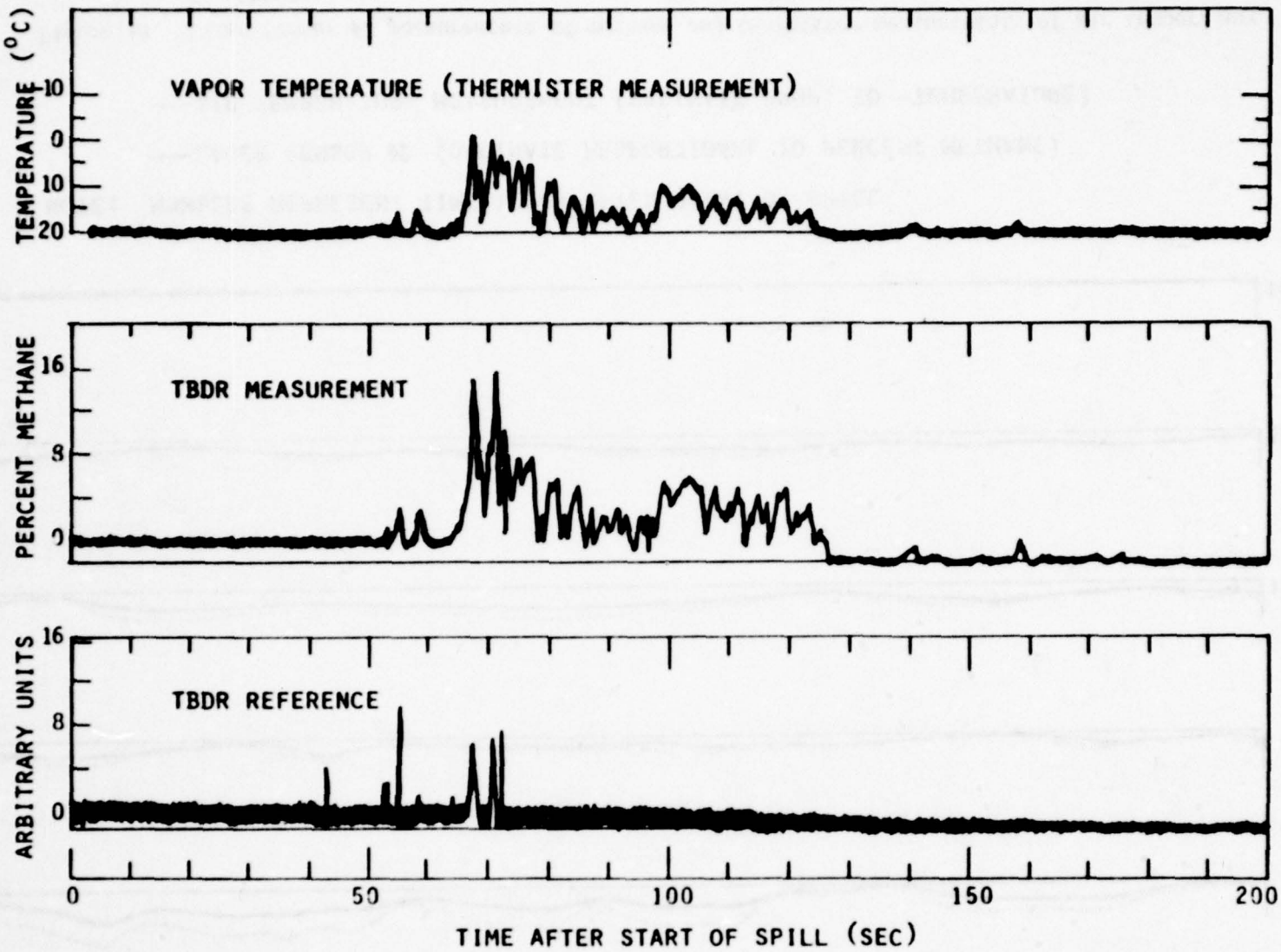

Figure 17. TBDR measurements of methane and thermister measurements of air temperature for LNG-21 Spill Test

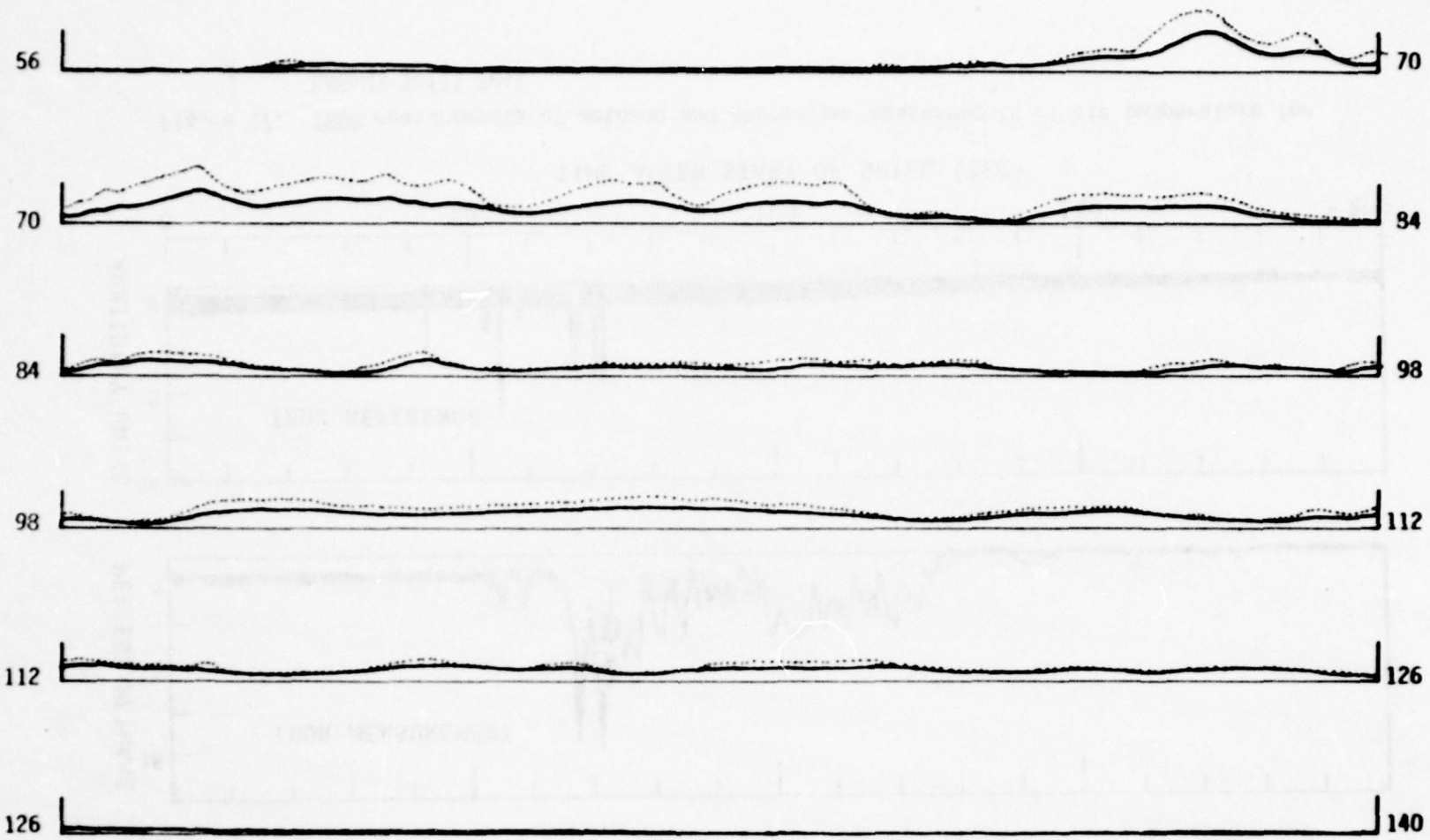

NOTE: NUMBERS REPRESENT TIME (SEC) AFTER START OF SPILL

——LASER SENSOR #2 (ORDINATE PROPORTIONAL TO PERCENT METHANE)

·····AIR TEMPERATURE MEASUREMENT (ORDINATE PROP. TO -TEMPERATURE)

Figure 18. Laser Sensor #2 measurements of methane and thermister measurements of air temperature for LNG-21

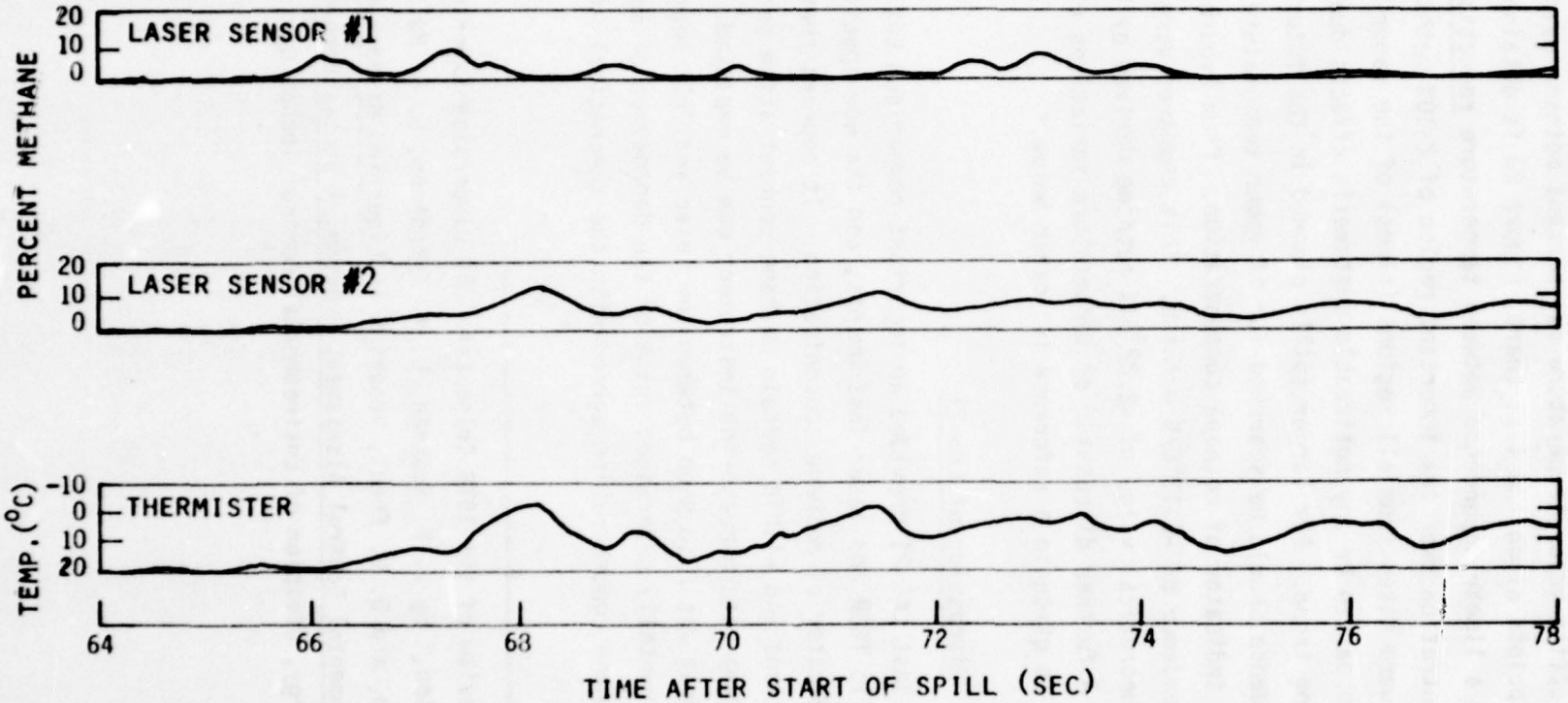

Figure 19. Laser sensor measurements of methane and thermister measurement of air temperature for LNG-21 Spill Test

By plotting vapor temperature vs. percent methane using data obtained at many points along the test chart, Figure 20 is obtained. There appears to be a linear dependence between temperature reduction and methane concentration over the important region of 2-10% methane; and, since data were taken from all regions (times) of the vapor cloud, there do not appear to be any noticeable systematic effects due to the overall cooling trend. For larger spills planned in the future, a systematic dependence should be searched for if vapor temperature is to be used as an indicator of methane concentration. From Figure 20 we calculate a dependence of -2.13°C/% methane. This compares very favorably with the theoretical value of -2.22°C/% methane derived by Lloyd Multhauf of LLL. A further discussion of temperature variations of the LNG vapor cloud is given in a reference indicated below.*

2.3.5 Discussion of LNG-21

Spill Test LNG-21 provided an important comparison between the species-specific TBDR and laser instruments, and the non-specific thermister as an indicator of methane concentration. It appears that, under certain conditions and within certain methane concentration ranges, an inexpensive temperature-measuring instrument can be employed. Good qualitative agreement was also seen between the laser and TBDR measurements; and the experimentally-determined value of the dependence of vapor temperature on methane concentration agreed with the theoretical value.

---

* "A Review of the 1978 China Lake LNG Dispersion Experiments and Instrumentation," by R. P. Koopman, L. M. Kamppinen, L. G. Multhauf, G. E. Bingham, and D. N. Frank, Report K in Liquefied Gaseous Fuels Safety and Environmental Control Assessment Program: A Status Report, U.S. Department of Energy, Division of Environmental Control Technology, May 1979.

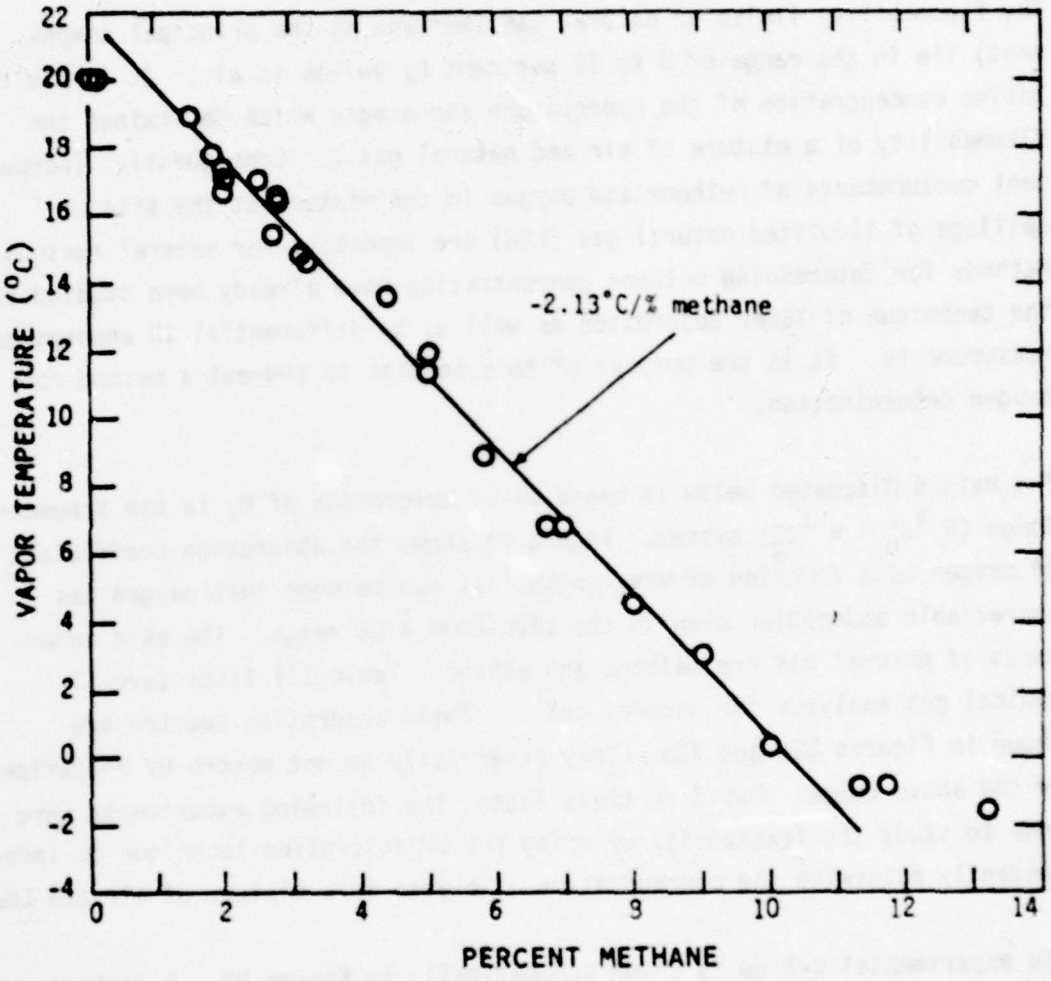

Figure 20. Plot of vapor temperature vs. percent methane for LNG-21

3. Laboratory Research

The following two investigations proceeded in parallel with the field program in order to evaluate future measurement capabilities.

3.1 Oxygen Monitoring Instrument

The flammability limits of natural gas (methane as the principal component) lie in the range of 5 to 15 per cent by volume in air. It is the relative concentration of the hydrocarbon and oxygen which determines the flammability of a mixture of air and natural gas . Consequently, independent measurements of methane and oxygen in the mixture at the site of spillage of liquified natural gas (LNG) are important for several reasons. Methods for determining methane concentration have already been studied by the technique of laser absorption as well as by differential IR absorption measurements. It is the purpose of this section to sugnest a method for oxygen determination.

The method discussed below is based on UV absorption of O_2 in the Schumann-Runge ($B\ ^3\Sigma_u^- - x\ ^3\Sigma_g^-$) system. Figure 21 shows the absorption coefficient of oxygen as a function of wavelength. It can be seen that oxygen has appreciable absorption even in the 1900-2000 Å UV range. The main components of natural gas are methane and ethane. Table III lists several typical gas analyses for natural gas . Their absorption spectra are shown in Figures 22a and 22b. They essentially do not absorb UV radiation in the above range. Based on these facts, the following experiments were done to study the feasibility of using the UV absorption technique to independently determine the concentration of oxygen in a mixture of air and LNG vapor.

The experimental set up is shown schematically in Figure 23. A deuterium lamp (Oriel Model 6312) is used as the source for UV radiation. The light from the lamp after collimation by a quartz condensing lens assembly (Oriel Model 6304) passes through a 1m long pyrex absorption cell. The cell is provided with two quartz windows for the incident and transmitted light, and also possesses inlet and outlet ports for the introduction of different gases. The transmitted radiation is focussed with a 20 cm focal length quartz lens (f/no. = 4) on the entrance slit of a 1/8 spectrometer (Oriel Model 7241). The monochromator has a 2400 ℓ/mm holographic

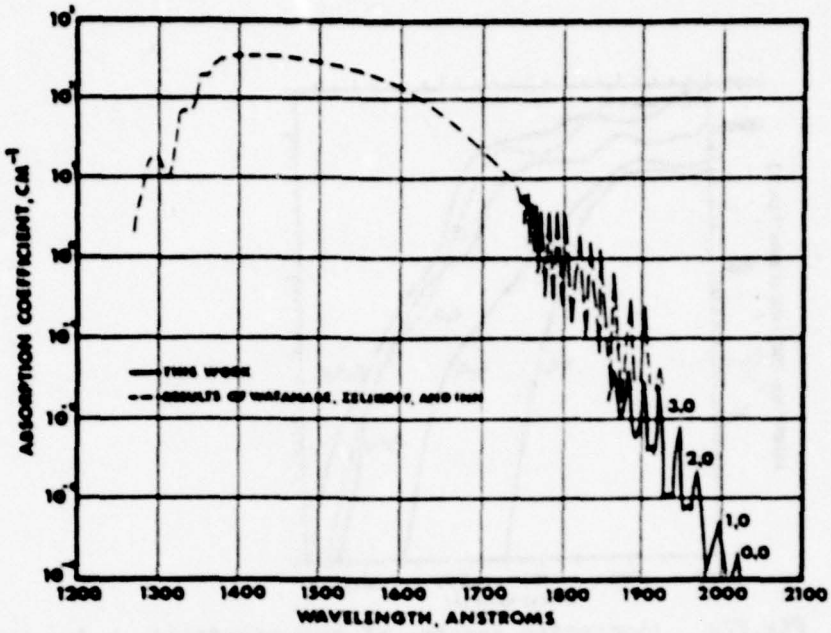

Fig. 21 Absorption coefficient of O_2 as a function of wavelength. (from B. A. Thompson et. al., J. Geophy, Res., 68, 6431 (1963))

TABLE III
Composition of Some Natural Gases
Per Cent of Various Components

Sample No.	CH_4	C_2H_6	N_2	CO_2	O_2	Heating Value Btu Per Cubic Foot* at 60 F and 30 in. Hg
1	88.92	3.20	7.68	0.16	0.14	959
2	81.91	17.51	0.11	0.31	0.16	1145
3	98.95	0.00	0.94	0.31	0.16	1000
4	82.86	16.51	0.16	0.31	0.16	1136
5	94.73	2.64	1.89	0.30	0.44	1008
6	66.31	31.70	1.21	0.47	0.31	1240
7	89.04	5.63	4.68	0.21	0.44	1004
8	90.52	4.56	4.29	0.21	0.42	1001
9	98.40	1.00	0.50	0.00	0.10	1016
10	82.60	7.20	7.10	2.70	0.40	967
11	74.20	18.50	7.30	—	—	1085
12	67.90	26.10	6.00	—	—	1157

* Calculated.

(from M. Popovich and C. Hering, Fuels and Lubricants, John Wiley & Sons, Inc., New York, 1969, 37 pp.)

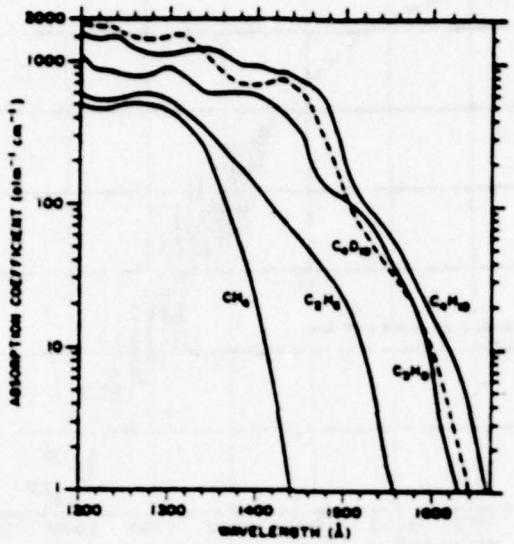

Fig.22a Absorption spectra of some paraffinic hydrocarbons: (from H. Okabe, and D. A. Becker, J. Chem. Phys., 39, 2549, (1963)

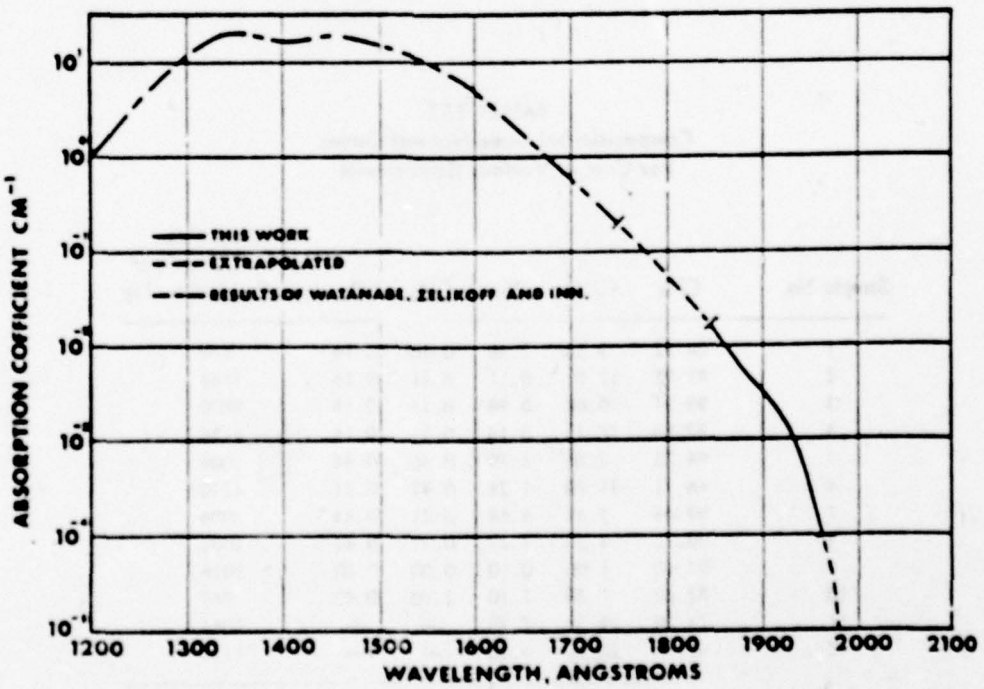

Fig. 22b Absorption coefficient of CO_2 as a function of wavelength. (from Thompson et. al.)

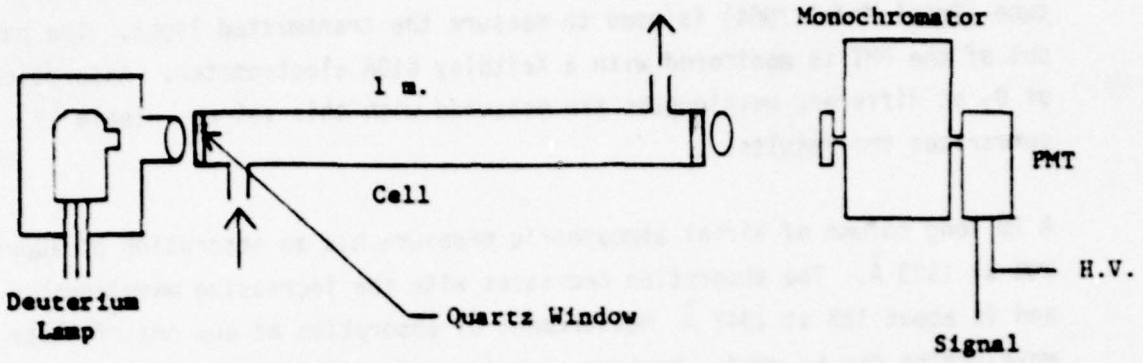

Fig. 23. Experimental Set up for Oxygen Measurement

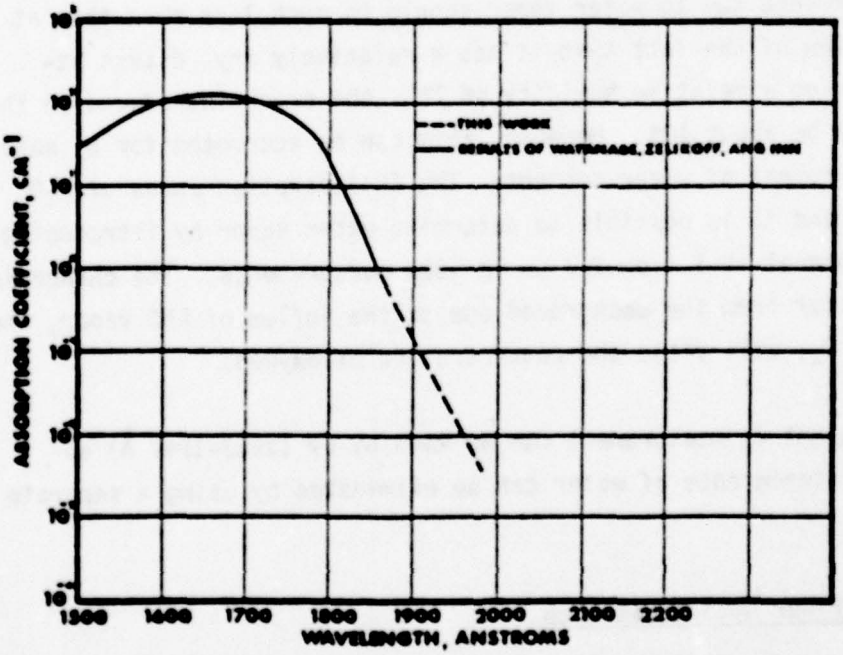

Fig. 24. Absorption coefficient of H_2O as a function of wavelength.
(from Thompson et al.)

grating blazed at 2000 Å (Oriel Model 7268). A solar blind photomultiplier tube (Oriel Model 7064) is used to measure the transmitted light. The output of the PMT is monitored with a Keithley 610A electrometer. Absorption of O_2 at different wavelengths are measured with this set up. Table IV summarizes the results.

A 1m long column of air at atmospheric pressure has an absorption of about 20% at 1923 Å. The absorption decreases with the increasing wavelength, and is about 12% at 1947 Å. Measurement of absorption at any one of these wavelengths can be used. However, consideration of interference from other gases suggests that 1947 Å may be the best choice. In particular, the absorption coefficient of CO_2 near 1947 Å is of the order of 10^{-4}; it, therefore, has negligible absorption. The absorption of CO_2 is not much different at 1923 Å. Thus CO_2 will not yield any major interference between 1923-1950 Å. The main interferant in the O_2 determination is water vapor, which has significant absorption in this wavelength region (Figure 24). Nitrogen saturated with water vapor at 1 atm pressure and at room temperature (partial pressure of water vapor of about 20 torr) in the absorption cell results in 4-5% attenuation in the incident light at 1947 Å. It is true that the interference due to water vapor should be much less than this at China Lake in view of the fact that it has a relatively dry, desert atmosphere. Assuming a relative humidity of 25%, the error introduced in the measurement will be about 10%. However, this can be accounted for by making a separate measurement of water content. The IR absorption bands of H_2O are well known, and it is possible to determine water vapor by introducing an additional channel at 1.4 or 2.7 μm in TBDR measurements. The change in the amount of water from the background due to the influx of LNG vapor, when subtracted from O_2, will yield the concentration of oxygen.

Thus, an independent O_2 measurement can be made by UV (1923-1947 Å) absorption. The interference of water can be eliminated by using a separate IR measurement.

3.2 Infrared Fiber Optics Research

Progress has been made since the preliminary results of the month of June 1978. During that time we computed the "numerical apertures" of the liquids

Table IV. Absorption measurements at several UV wavelengths for dry air, oxygen, and nitrogen saturated with water vapor at room temperature.

	Percent Absorption		
λ (Å)	DRY AIR	OXYGEN	WATER-SATURATED N_2
1923	20	60	11
1947	12	40	4
1971	4	--	1

Carbon Tetrachloride ($CC\ell_4$) and Tetrachloroethylene ($C_2C\ell_4$) at the wavelength of 3.39 μm, and also the maximum angles of acceptances. We concluded $C_2C\ell_4$ to be a better candidate for the liquid-core fiber. *

Since then we have modified the optical system design as follows:

i) We have used a Spectra Physics He-Ne laser, Model 124/B operating at 3.39 μm wavelength with a power output of 6 mWatts (measured). This increased the signal at the output of the fiber to an easily-detectable level.

ii) We used an Indium Arsenide detector (Judson Infrared), which operates with much improved sensitivity, compared to pyroelectrics. This is one of the few infrared detectors which has peak responsivity at around 3.4 μm, the wavelength at which we are operating.

iii) A smaller size hypodermic needle (#26g) was used, This enabled the quartz fiber to be straighter while inside the window system.

iv) We have incorporated a micropositioner in the system to hold the window-fiber assembly for both the input and the output ends of the fibers. In this way we can precisely adjust the penetration of the laser light into the fiber waveguide as well as fine-position the output end of fiber to get maximum signal.

With the modifications in the experimental set up described above, the transmission loss in the liquid-core hollow fibers was measured. The liquid was tetrachloroethylene ($C_2C\ell_4$). The output of the fiber end was measured by the InAs detector. The detected output signal was measured as a function of the fiber length by cutting successive pieces from the original 16-meter length. The results are shown in Figure 25. The data points with NG-1 and NG-3 filters were taken to measure the losses with attenuated laser light. From the slope of the curve, we calculated the transmission loss of this liquid-core fiber to be 56.2 db/km.

---

* For a scientific publication based upon this research, see "Infrared Transmission at the 3.39 μm Helium-Neon Wavelength in Liquid-Core Quartz Fibers," by A. K. Majumdar, R. T. Menzies, and E. D. Hinkley, Journal of Quantum Electronics (June 1979).

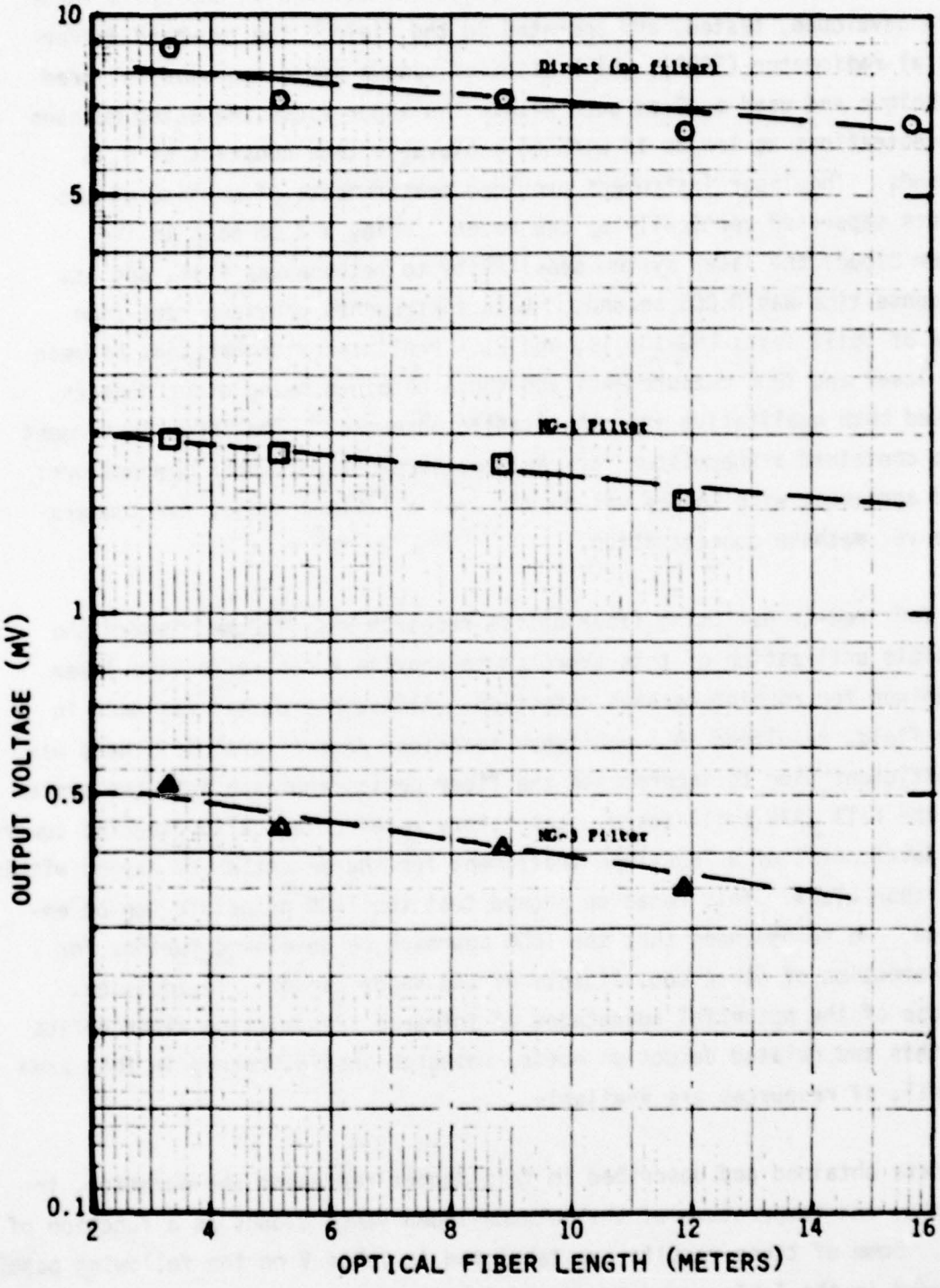

Figure 25. InAs detector signal for various fiber optics lengths and laser power levels

4. Conclusion and Tabulation of Results

Two types of instruments for the detection of methane in LNG spill vapor were developed, tested, and operated in the field. The two-band differential radiometer (TBDR), which is based upon a non-dispersive infrared technique and used a 20 cm path within the vapor cloud, detected methane concentrations as low as 1% with an achievable time constant of 0.15 seconds. The laser instrument provided measurements of methane at two points separated vertically by one meter. Using a 2 cm path in the vapor cloud, the laser system sensitivity to methane was 0.1%, and its response time was 0.005 seconds. Both instruments provided real-time data of Spill Tests LNG-18, 19, and 21. Preliminary comparisons between the laser and TBDR measurements and those obtained using other sensors, showed both qualitative and quantitative agreement. The laser instrument also contained a thermister for rapid measurements of vapor temperature; good agreement with theory was found, over a limited range, for temperature vs. methane concentration.

The infrared-transmitting fiber optics research was directed toward the possible utilization of this approach to provide a cost-effective laser technique for routine methane detection. Although progress was made in this field, resulting in a published technical journal article, there was insufficient time to incorporate the fiber optics approach into the system for the Fall 1978 spill tests. Laboratory research was also directed toward the development of a TBDR-type instrument for the detection of oxygen within the vapor cloud. This research showed that the TBDR principle can be employed. We recommended that the TBDR approach be developed further for the detection of other constituents of LNG vapor clouds. In addition, because of the potential advantages of infrared transmitting fiber optics for this and related detection needs, research should proceed in this area as well, if resources are available.

The data obtained and described in this Report represent the duration, intensity, and temperature of the methane-laden vapor clouds as a function of time. Some of these results are tabulated in Table V on the following page. Included in the Table are data on the fraction of time the methane concentration exceeded 5%.

Table V. Summary of Results of Spill Tests

	LNG-18		LNG-19		LNG-21	
	1.5 m	2.5 m	1.5 m	2.5 m	1.5 m	2.5 m
First Vapor Cloud						
Time from spill (sec):	40.2	40.2	40.4	40.4	57.2	57.2
Duration (sec):	4.6	2.4	1.5	1.0	1.5	0.3
Peak CH_4 conc. (%):	10.9	11.1	1.28	0.28	3.8	1.8
Time above 5% CH_4 (%):	30.	26.	0	0	0	0
Second Vapor Cloud						
Time from spill (sec):	61.4	61.4	93.2	95.0	64.2	64.2
Duration (sec):	41.0	39.4	3.8	1.0	63.2	61.7
Peak CH_4 conc. (%):	14.2	11.4	1.46	0.44	13.5	11.9
Time above 5% CH_4 (%):	35.	6.3	0	0	27.	8.
Third Vapor Cloud						
Time from spill (sec):			105.2	105.2		
Duration (sec):			0.12	0.28		
Peak CH_4 conc. (%):			0.12	0.14		
Time above 5% CH_4 (%):			0	0		

Note: The 1.5 m and 2.5 m column headings refer to the height of the sensor above the ground.

5. Acknowledgments

The following individuals at JPL contributed to this Program: C. Giffin, R. H. Green, G. Hawkes, E. D. Hinkley, A. Majumdar, R. T. Menzies, N. Miller, D. Norris, J. Peterson, G. Reisdorf, D. R. Rupnik, C. Rutledge, M. S. Shumate, N. K. Simon, M. P. Sinha, J. Riccio, and R. A. Zanteson.

We are indebted to Doug Lind of the China Lake Naval Weapons Center for his assistance in performing these spill tests. We also express appreciation to the Lawrence Livermore Laboratory personnel for use of their trailer for the JPL data recording system and for general support. In particular, we thank Ron Koopman for providing LLL data for LNG-18 quoted in this Report.

This Program was supported in part by the U.S. Coast Guard, the American Gas Association, the Gas Research Institute, the Department of Energy, and the National Aeronautics and Space Administration. This Report represents one phase of research carried out at the Jet Propulsion Laboratory, California Institute of Technology, under contract NAS 7-100, sponsored by the National Aeronautics and Space Administration.

APPENDIX A

Principles of Operation of TBDR System

The principle underlying the TBDR design concept is that the gas of interest absorbs strongly in one wavelength band and not at all in another band; that other gases present don't absorb preferentially in either of the two selected bands; and that particles (dust, aerosols, ice crystals, water droplets, etc.) don't completely extinguish the light being measured. If the two spectral bands are close together, particle scattering will be similar in both bands.

Figure A-1 schematically depicts the TBDR sensor. Broad-band light is generated by a small lamp and is collimated by Lens #1. The absorbing volume consists of the space between Lens #1 and Lens #2. The light which passes through the absorbing gases is collimated and split by a beam splitter (in this case a partially silvered mirror) to image the light on two different detectors: D1 and D2. By this arrangement, the absorption path is identical for D1 and D2 channels, and anything that transpires in this volume can be simultaneously measured by the two detectors. Filters F1 and F2 are used to select the appropriately absorbing and non-absorbing spectral bands. The following analytical discussion is intended to show that the measured properties of atmospheric and LNG gases allow a simple implementation of the TBDR and provide a measurement method satisfying the needs of the Spill Test Program.

The attenuation of light by molecular absorption and particle scattering (assuming single scattering theory applies) is governed by the Beer-Lambert equation:

$$I = I_0 e^{-\epsilon c L} \qquad (1)$$

where:

I = Light intensity at observing position

I_0 = Unattenuated light intensity

ϵ = Extinction coefficient

$\epsilon = \alpha + s$

α = Molecular absorption coefficient

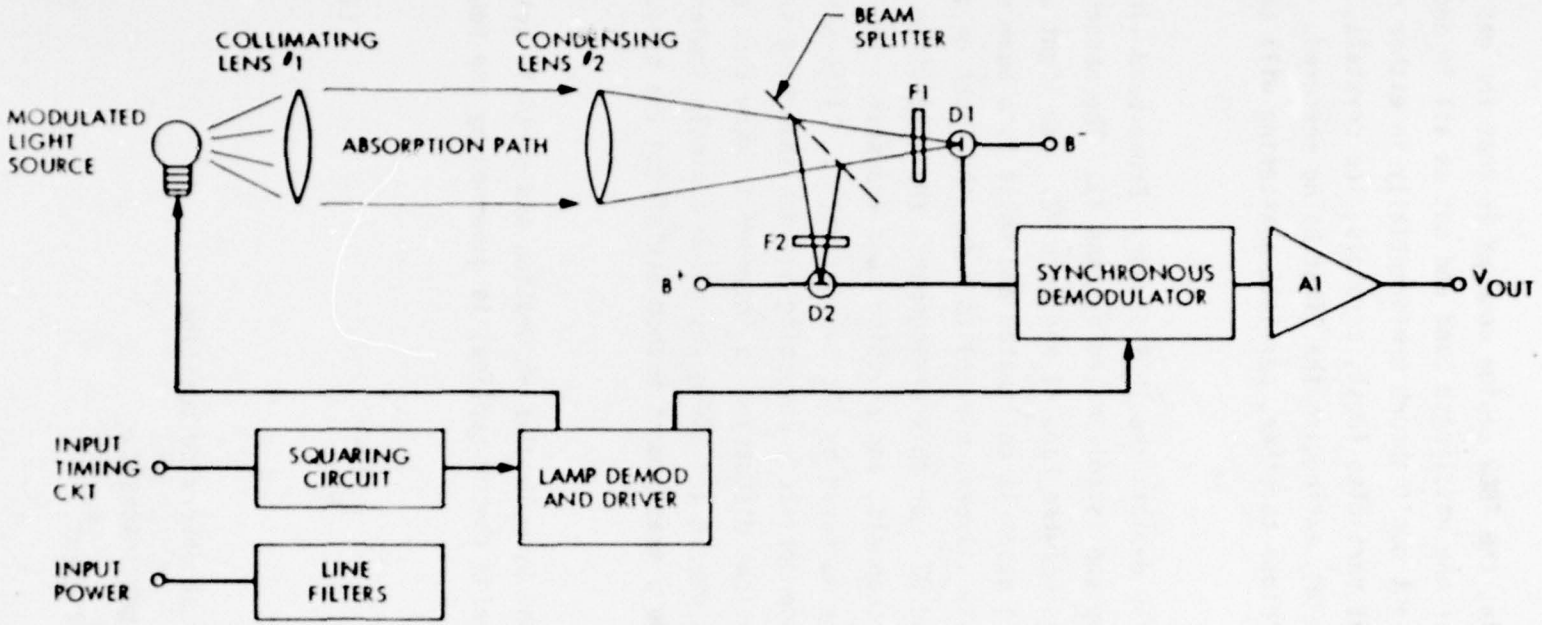

F1, F2: Spectral Filters

D1, D2: Detectors

A1: Amplifier

Fig. A-1. Block Diagram for TBDR Sensor Module, showing integration of optics and electronics

s = Scattering coefficient

L = Absorbing path length

c = Concentration of gas or particles

Two options in configuring the system are to ratio the outputs of the two detectors or to difference the output of the two detectors. In the ratio case,

$$\frac{I_1}{I_2} = e^{-c(gas)L(\alpha_1 - \alpha_2)-c(particle)L[S_1 - S_2]}. \quad (2)$$

As will be shown later, the spectral bands proposed are close enough that scattering coefficients will be approximately the same, so that $S_1 - S_2 = 0$ and

$$\frac{I_1}{I_2} = e^{-cL[\alpha_1 - \alpha_2]}. \quad (3)$$

A linear display of the absorbing gas concentration (c) can be obtained by plotting the negative natural log of the two-channel outputs:

$$\left[\frac{-\ln \frac{I_1}{I_2}}{(\alpha_1 - \alpha_2)}\right] = c. \quad (4)$$

The ratio approach is elegant from the standpoint of Equation (4) but is considerably more complex than the two-channel difference method.

Appendix D contains measured spectra of methane, ethane, propane, butane, water vapor, oxygen, nitrogen, and carbon dioxide. From these spectra it can be deduced that an absorption cell of a few centimeters length operating at 2.1 μm and 2.3 μm will allow measurements of the LNG constituents without significant interference from other gases.

To avoid problems such as background light and detector bias offset, the light source is driven by an A/C source, and the A/C signal is then synchronously detected and amplified by A_1 to give a large signal which is

transmitted to the central recorder. Commercial lamps are available that can be modulated at 100 Hz, and PbS (lead sulfide) detectors have peak detectivity at 100 Hz.

The squaring circuit gives high noise immunity to any pickup on the input lines, and the following lamp and demodulator driver is a simple power amplifier. In addressing the problem of temperature compensation and thermal calibration, the most economical approach in time and dollars appears to be to temperature control the sensor slightly above ambient temperature using a simple "bang-bang" heater and attendant sensor and controller. In looking ahead to possible large-scale production of TBDR's, it should be noted that all of the electronics in the sensor can be built in one Large Scale Integrated Circuit Chip (LSI) of modest complexity.

APPENDIX B

Principles of Operation of Laser System

This appendix describes the operating principles of the laser system used during the August-November, 1978 spill tests at China Lake. A single-frequency 3.39 μm helium-neon laser, with a few milliwatts output power, was used. The infrared frequency of this laser overlaps that of a strong methane spectral line, as shown in Fig. B-1. Laboratory tests using several different mixing ratios of methane in nitrogen yielded an absorption coefficient of 8.8 ± 0.1 cm^{-1} atm^{-1} at room temperature. This result compares favorably with the value of 8.9 ± 0.3 cm^{-1} atm^{-1} obtained by averaging values of Gerritsen (1966), Kucerovsky (1973), and Pine (1975).

Transmission of a laser beam of power P_o along a path of length L containing a gas with absorption coefficient α' is given by the following expression:

$$P = P_o \exp(-\alpha' cL). \qquad \text{(B-1)}$$

P is the power at the end of the path, and c is the average gas concentration. For a methane concentration of 5% (c = 0.05 atm) and a pathlength of 2 cm, the transmittance (P/P_o) is calculated to be 0.41 -- an easily-measurable value.

There are several aspects of laser monitoring which must be considered as (potentially) contributing to measurement errors:

a) Self-Broadening of the Methane Absorption Line

The air-broadening coefficient for a methane absorption line in the 3.4 μm region is approximately 4.5 MHz/torr, whereas, that for self-broadening may be as high as 7.4 MHz/torr. Consequently, when the methane concentration becomes a significant fraction of the total gas present, the absorption line will be broader, resulting in a decrease in the absorption cross section. (Usually there can be exceptions depending on where the laser line is located relative to absorption line center.) Figure B-2 illustrates the percent transmission of the helium-neon laser line at 3.3922 μm vs. percent methane

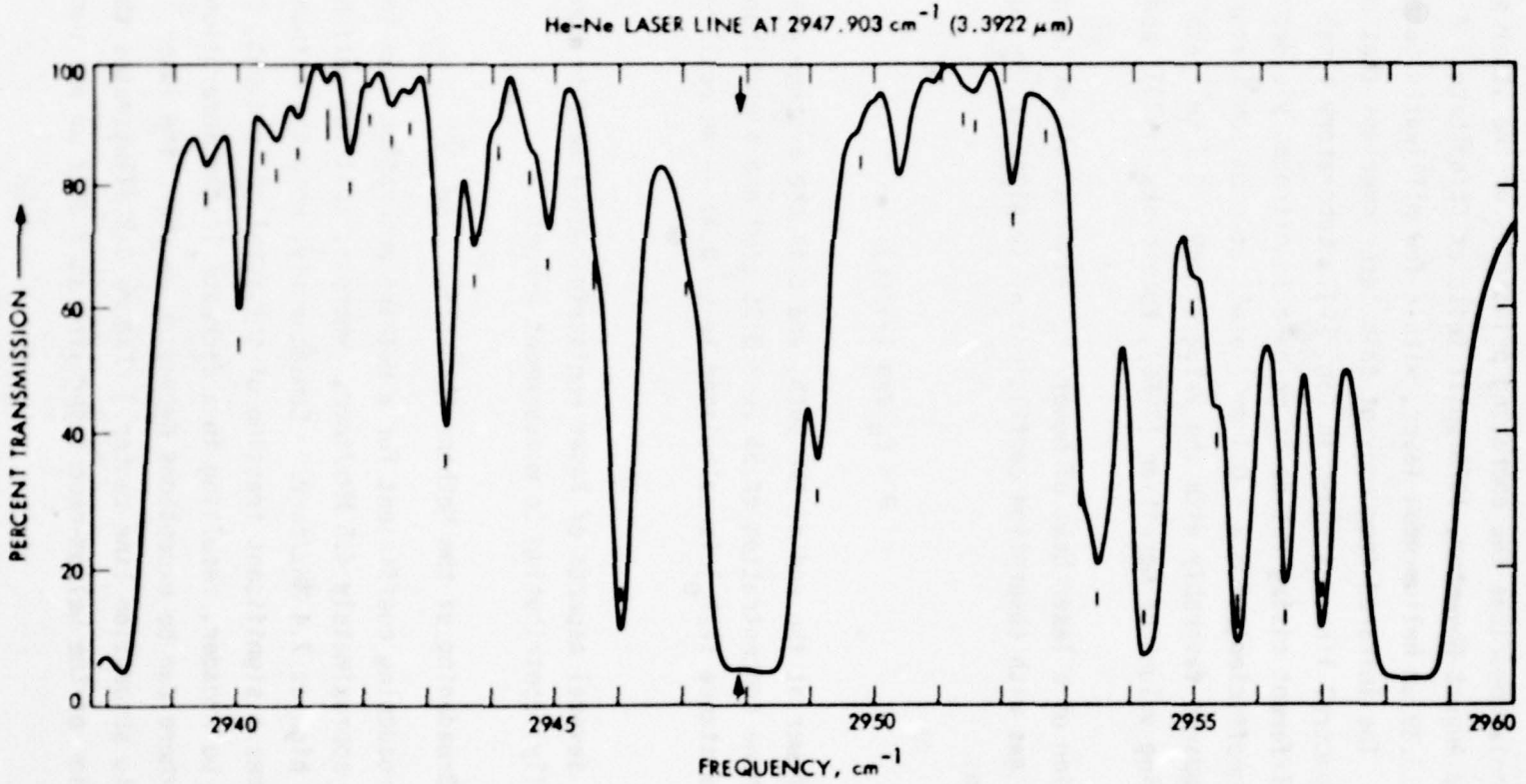

Fig. B-1. Methane spectrum around 3.39 μm, with helium-neon laser frequency indicated.

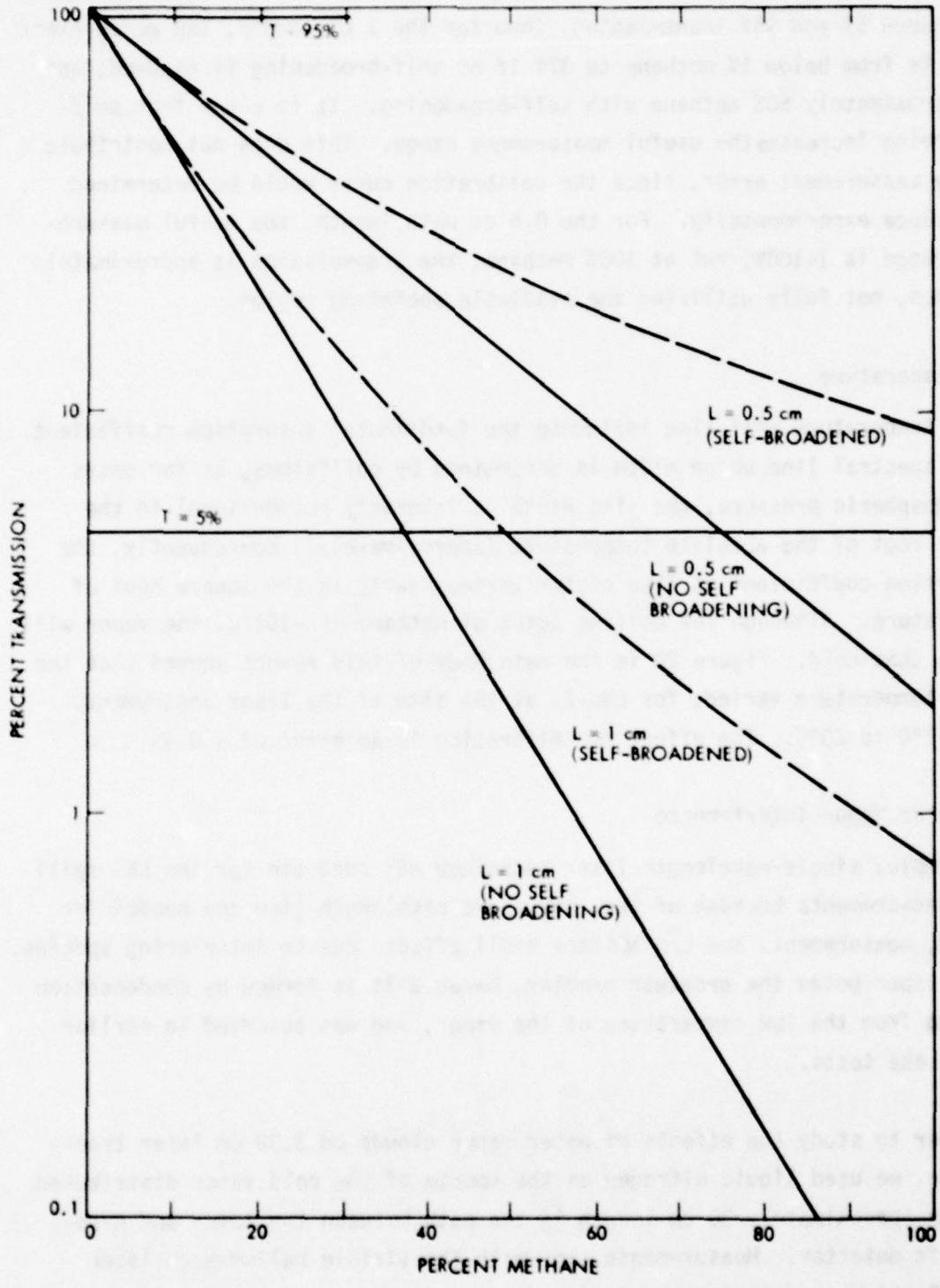

Fig. B-2. Percent Transmission of 3.3922-μm laser radiation through two different pathlengths of methane/air mixtures from zero to 100% (theoretical curves).

for two specimen lengths (1 cm and 0.5 cm), for the case of no self-broadening, and with self-broadening. If we expect the greatest measurement accuracy to be between 5% and 95% transmission, then for the 1 cm length, the measurement range is from below 1% methane to 37% if no self-broadening is assumed, and to approximately 50% methane with self-broadening. It is clear that self-broadening increases the useful measurement range. This does not contribute to any measurement error, since the calibration curve would be determined in advance experimentally. For the 0.5 cm path length, the useful measurement range is 1-100%; but at 100% methane, the transmission is approximately 9%, thus, not fully utilizing the available operating region.

b) Temperature

Vapor temperature will also influence the fundamental absorption coefficient. For a spectral line whose width is determined by collisions, as for gases at atmospheric pressure, the line width is inversely proportional to the square root of the absolute temperature (approximately); consequently, the absorption coefficient at line center varies nearly as the square root of temperature. Although the boiling point of methane is -162°C, the vapor will not be that cold. Figure 20 in the main body of this report showed that the vapor temperature varied, for LNG-21 at the site of the laser instrument, from -2°C to 20°C. The effect on calibration is an error of < 0.4%.

c) Water Vapor Interference

The simple, single-wavelength laser technique was adequate for the LNG spill test measurements because of the very short pathlength (few cm) needed for the CH_4 measurement, and concomitant small effects due to interfering species. Water vapor poses the greatest problem, because it is formed by condensation arising from the low temperature of the vapor, and was observed in earlier China Lake tests.

In order to study the effects of water vapor clouds on 3.39 μm laser transmission, we used liquid nitrogen as the source of the cold vapor distributed over an approximately 30 cm length in the path between the laser and pyroelectric detector. Measurements made with the visible helium-neon laser (0.6328 μm) showed that transmission dropped to near zero in the presence of the water vapor "cloud". The results of the infrared laser measurements

for three different "clouds" are shown in Figure B-3. The maximum effect on transmission due to these "clouds" was to reduce it to a value of around 30%. This corresponds to a systematic error in the calculated CH_4 concentration of + 0.5%, independent of the pathlength used. It must be stressed, however, that this water vapor cloud is considerably more dense than that existing in the LNG spill tests (since it was generated by the 77K temperature of liquid nitrogen, vs. the 110K temperature of LNG). Consequently, water vapor interference is expected to be negligible.*

d) Laser Noise

Noise induced by changes in laser power or frequency with time can limit the minimum detectable signal. In terms of frequency, the 3.39 μm line of the helium-neon laser is extremely stable, and should not cause any noticeable degradation of performance, especially since the spectral line being monitored is broadened by atmospheric-pressure collisions.

e) Infrared Detector Temperature Dependence

Because of the range of temperature for the LNG vapor, consideration must be given to the temperature dependence of the infrared detectors employed. Pyroelectric detectors are notoriously temperature sensitive, and for this reason, were not selected for the China Lake tests. InAs photovoltaic detectors were chosen for the laser system because of their high sensitivity and relatively low cost.

f) Error Analysis

The discussions above relate to achieving the minimum detectable signal during the laser measurements. On the basis of other types of laser measurements in which signal detection limits of 0.3% to 1% have been achieved in field application using short time constants, it is not unreasonable to assume that we will be able to detect, with high accuracy, signals corresponding to transmission in the 5%-95% region. If we can measure over this range with 10% accuracy (of the reading), then from Figure B-2, using a 1 cm path length, the methane concentration range which can be accurately monitored is < 1%-50% (assuming self-broadening at 7.4 MHz/torr). For a 1% methane concentration,

---

* NOTE: Water vapor interference would yield a CH_4 concentration which was too high. This was not observed to be the case for any of the spill tests.

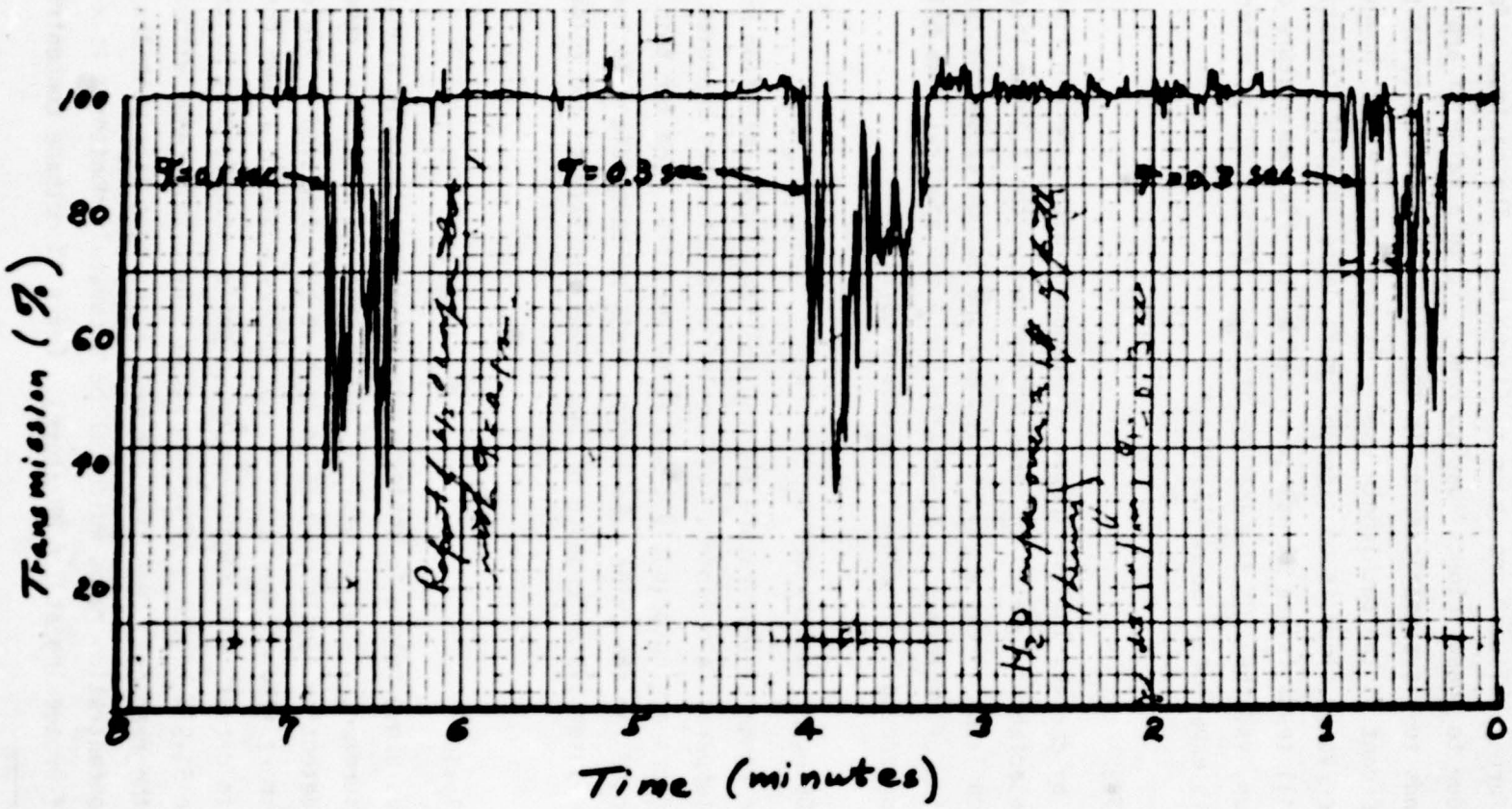

Figure B-3. Effect of water vapor on transmission at 3.39 um wavelength. Water vapor attenuates visible-wavelength radiation to zero for this test.

the measurement error will be ± 0.1%; for 50%, the error will be ± 5%. Measurements can be made beyond this range, but the accuracy will be somewhat lower for methane concentrations approach 100%. The signal processing schematic for the Laser System is shown on Figure B-4, and the electronics schematics in Figs. B-5, B-6, and B-7.

References for Appendix B

Gerritsen, H. J., "Methane Gas Detection Using a Laser," Trans. Soc. Mining Engineers, 428 (December 1966).

Z. Kucerovsky, E. Brannen, K. C. Paulekat, and D. G. Rumbold, "Characteristics of a Laser System for Atmospheric Absorption of Air Pollution Experiments," J. Applied Meteorology, 1387 (December 1973).

A. S. Pine, "Tunable Laser Spectral Survey of Molecular Air Pollutants," Progress Report from MIT Lincoln Laboratory to the National Science Foundation, November 1975.

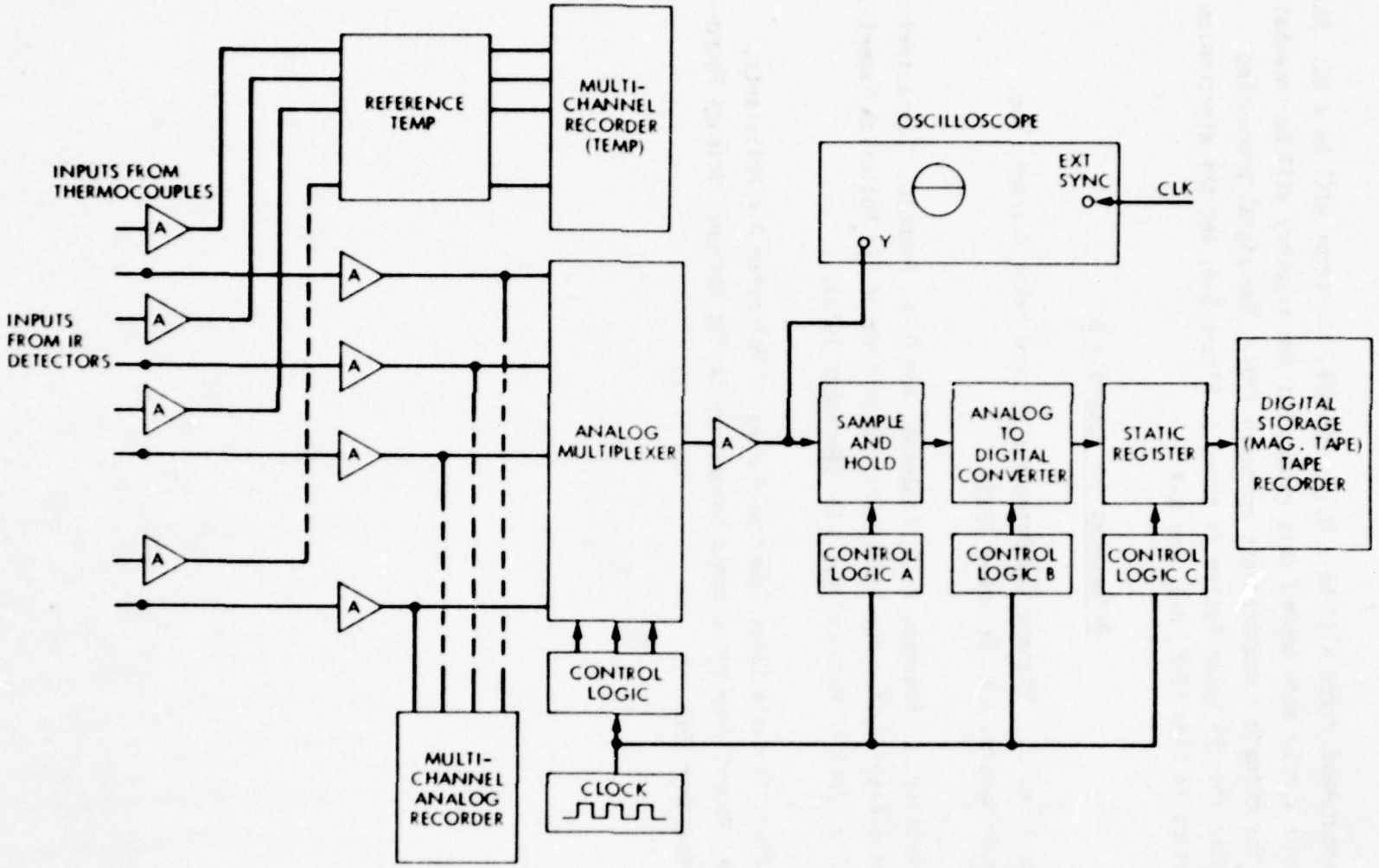

Fig. B-4 Laser System signal processing and storage scheme.

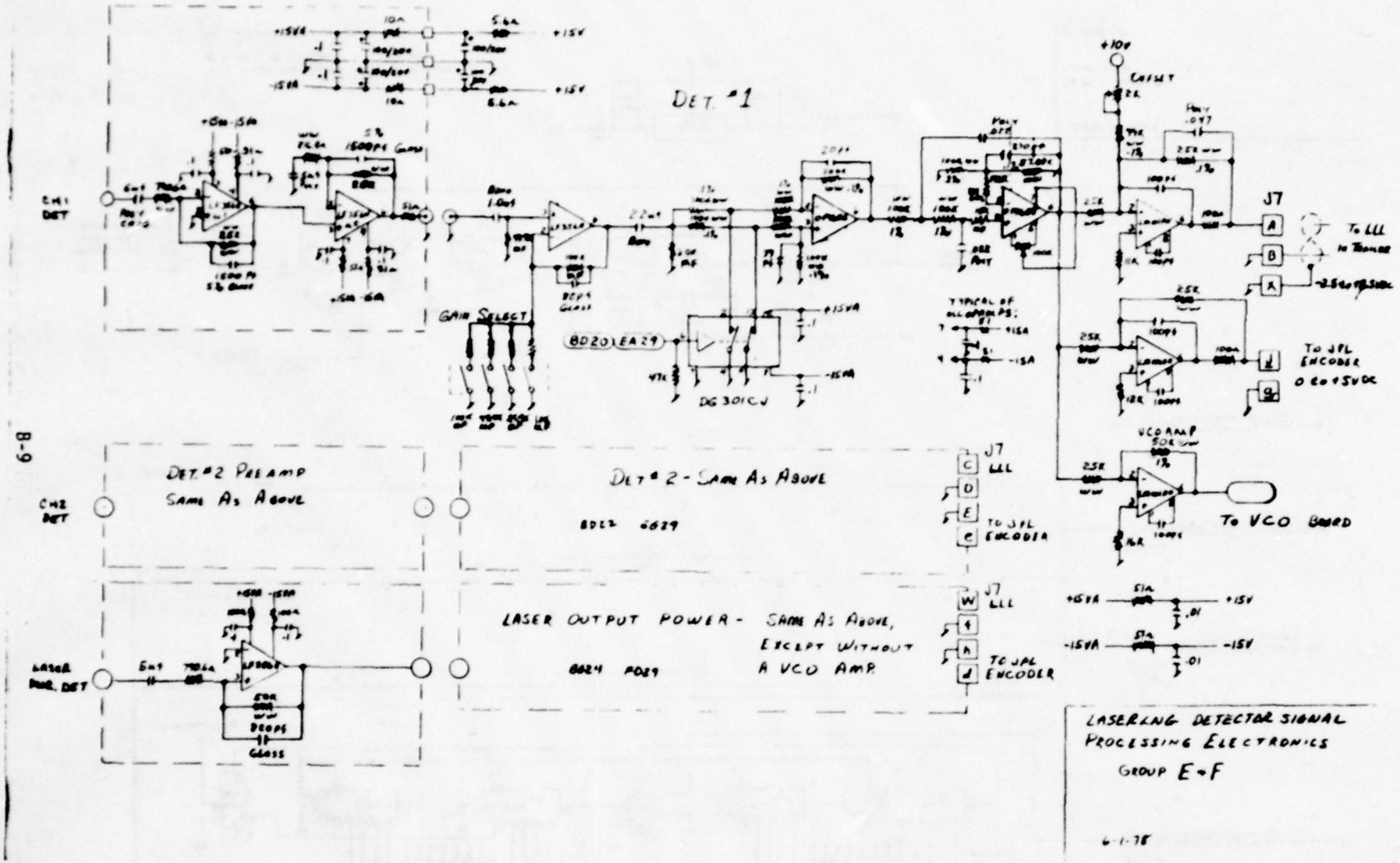

Fig. B-5. Laser detector signal processing electronics.

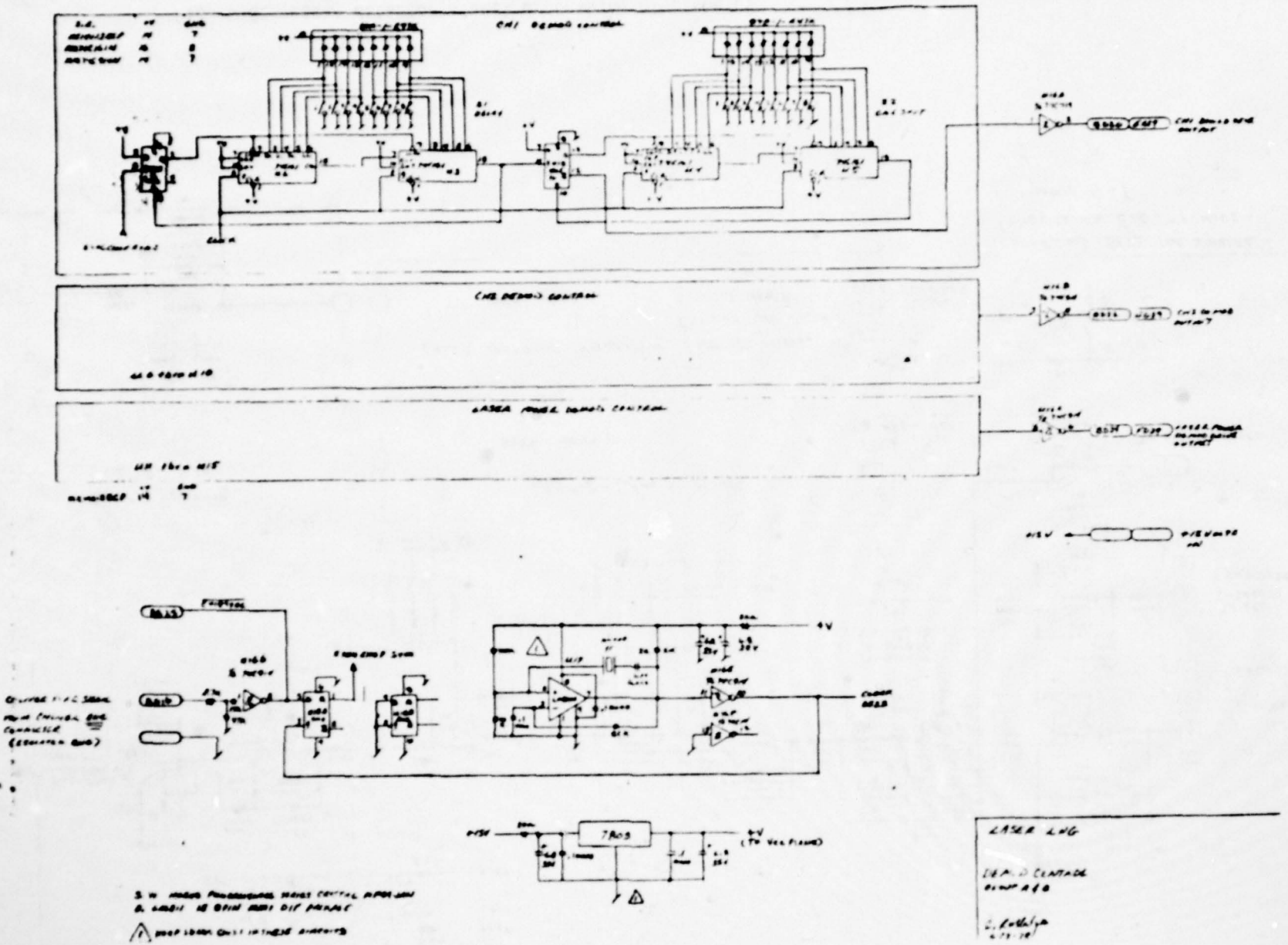

Fig. B-6. Laser system demodulator control circuit

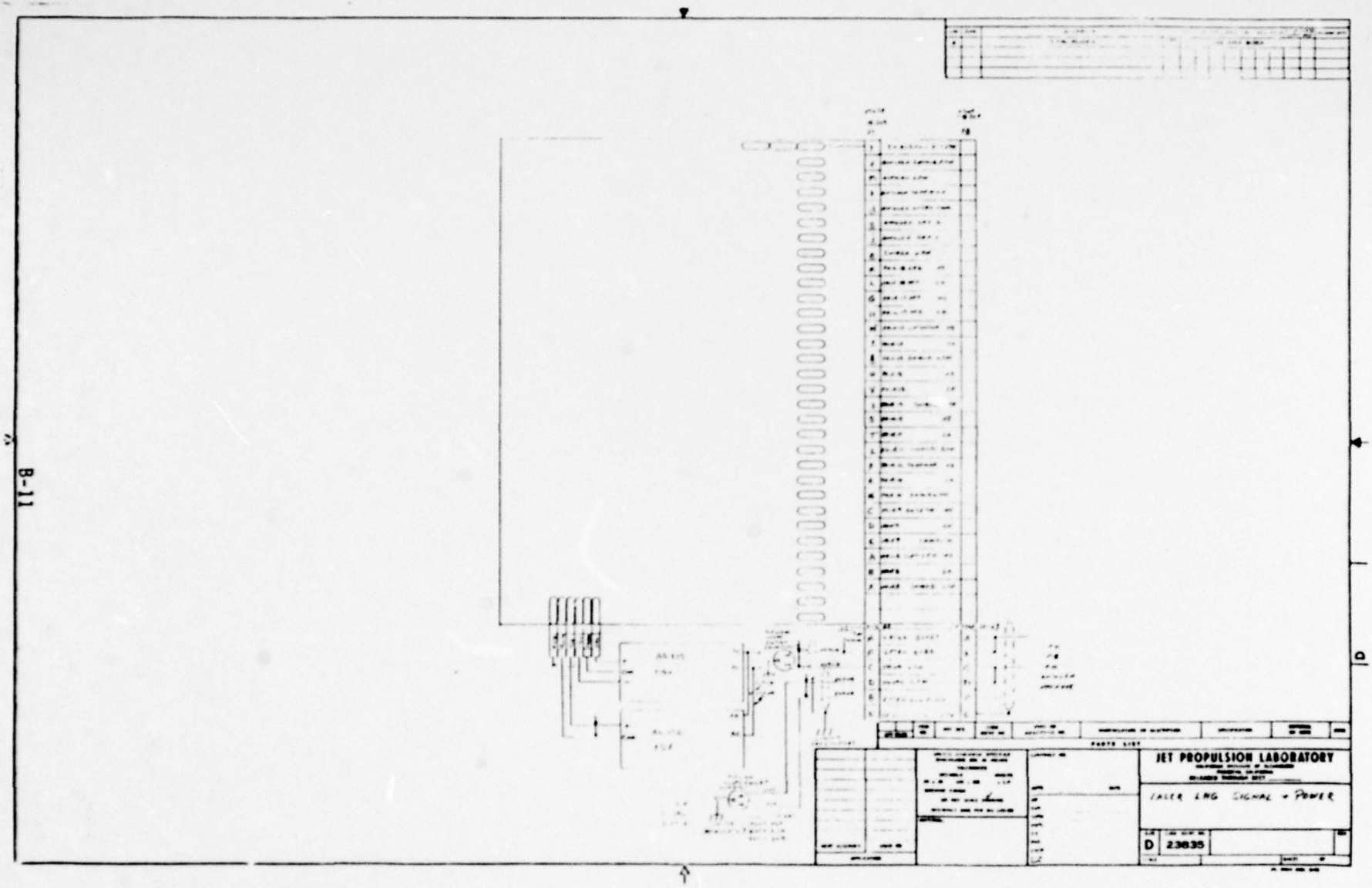

Fig. B-7. Laser system signal and power connections.

APPENDIX C

Principles of Temperature Monitoring

The LNG Temperature Multiplexer is design to record the vapor cloud temperature, the temperatures in the vicinity of the three infrared detectors, and the temperature within the laser instrument. The multiplexer produces these data in a sequential manner: Two pulses are superimposed on the data to signify the beginning of Channel 1, and a single pulse occurs each time the multiplexer switches to succeeding channels. The sequence is: Detector 1, Detector 2, laser power, and cloud temperature, which corresponds to Channel 1, 2, 3, 4, respectively. The laser system interior temperature was measured using an ohmmeter, and was not connected to the multiplexer for the Fall 1978 spill tests.

Since the laser power detector and the two signal detectors are temperature sensitive, a large thermal capacity was designed into their mounts. This minimized the short-term thermal effects which might otherwise be induced by the LNG vapor cloud. The actual detector temperatures were monitored by linearized thermistor networks, Model (YSI-44211A); and the temperature multiplexer contains circuitry needed to translate the thermistor signals into linear (50 mV/°C) outputs for data recording.

The inside air temperature of the laser instrument was monitored by a YSI-44033 thermistor. This thermistor permits the operator to deactivate the instrument if the laser operating temperature limits are exceeded.

The location of the air-temperature thermistor is shown in Fig. 8 in the main body of this Report. This thermistor monitors the temperature of the vapor cloud. The criteria used in selecting this thermistor were small physical size and the ability to withstand the anticipated environment. Since a fast response time ($\sim$ 0.1 - 0.2 sec) was desired, the linearized thermistor network was not used in this case (its response time is $\sim$ 10 sec). 0.36 mm (0.014") diameter pre-mounted glass-coated bead thermistor, Fenwall GB38T1, was used. The temperature multiplexer contains circuitry for con-

verting the nonlinear resistance-temperature characteristic of the thermistor to a nearly linear output voltage with a time constant of $\sim$ 0.2 sec. Useful data may be obtained over the range from -60°C to +60°C, with best linearity occurring between -40°C and +30°C. In order to prevent electrical leakage due to moisture, the uninsulated thermistor leads were coated with a thin layer of insulating varnish (GC Print-Kote #14-2). The thermistor, along with its integral mount, was installed inside a protective housing and mounted on the instrument, as shown in Fig. 8. The electrical schematic for the temperature-monitoring system is given in Fig. C-1.

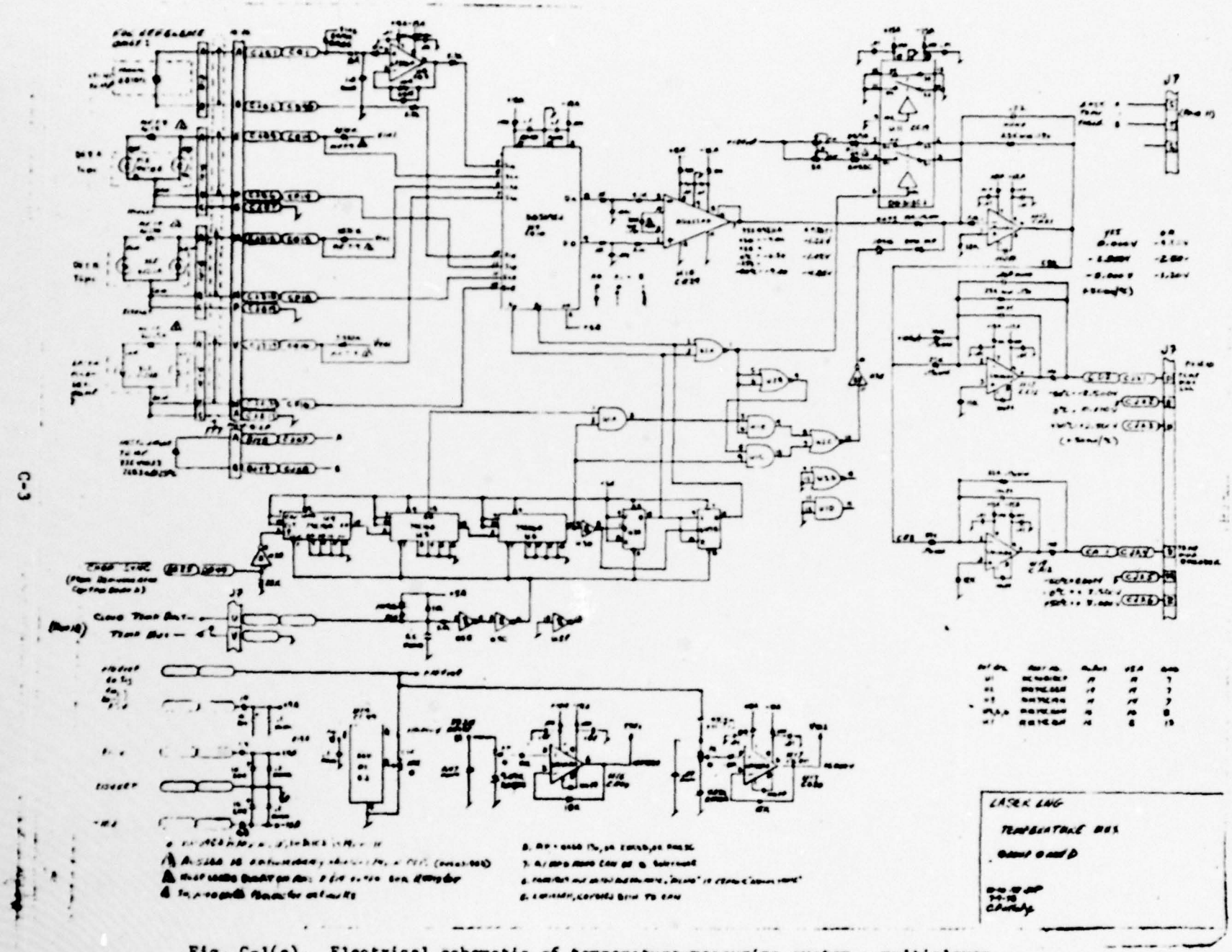

Fig. C-1(a). Electrical schematic of temperature-measuring system - multiplexer

APPENDIX D

Measured Spectra in the 0.3-2.5 μm Region of Several Gases Important to LNG Vapor Monitoring and Background Interferences

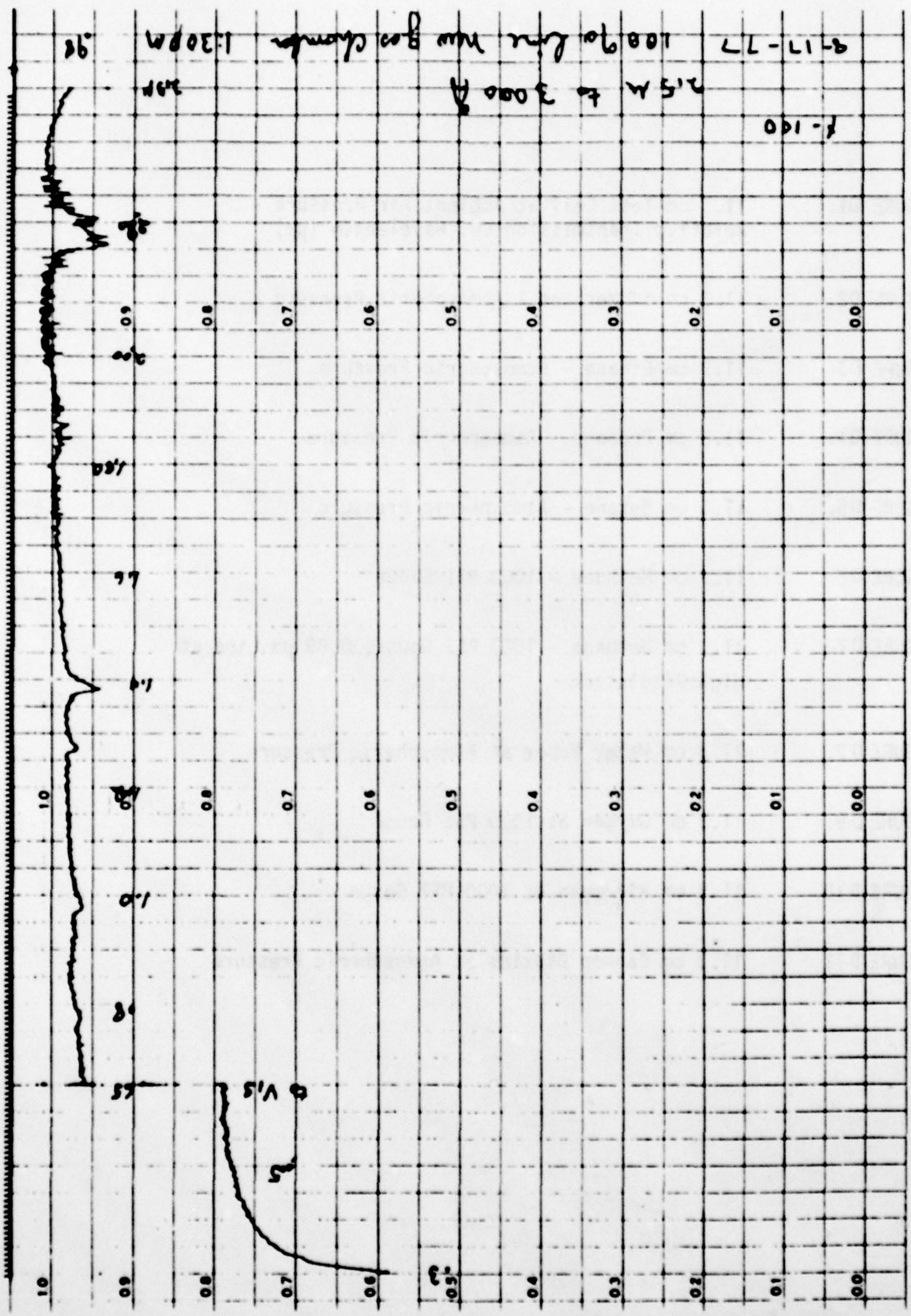

Fig. D-1

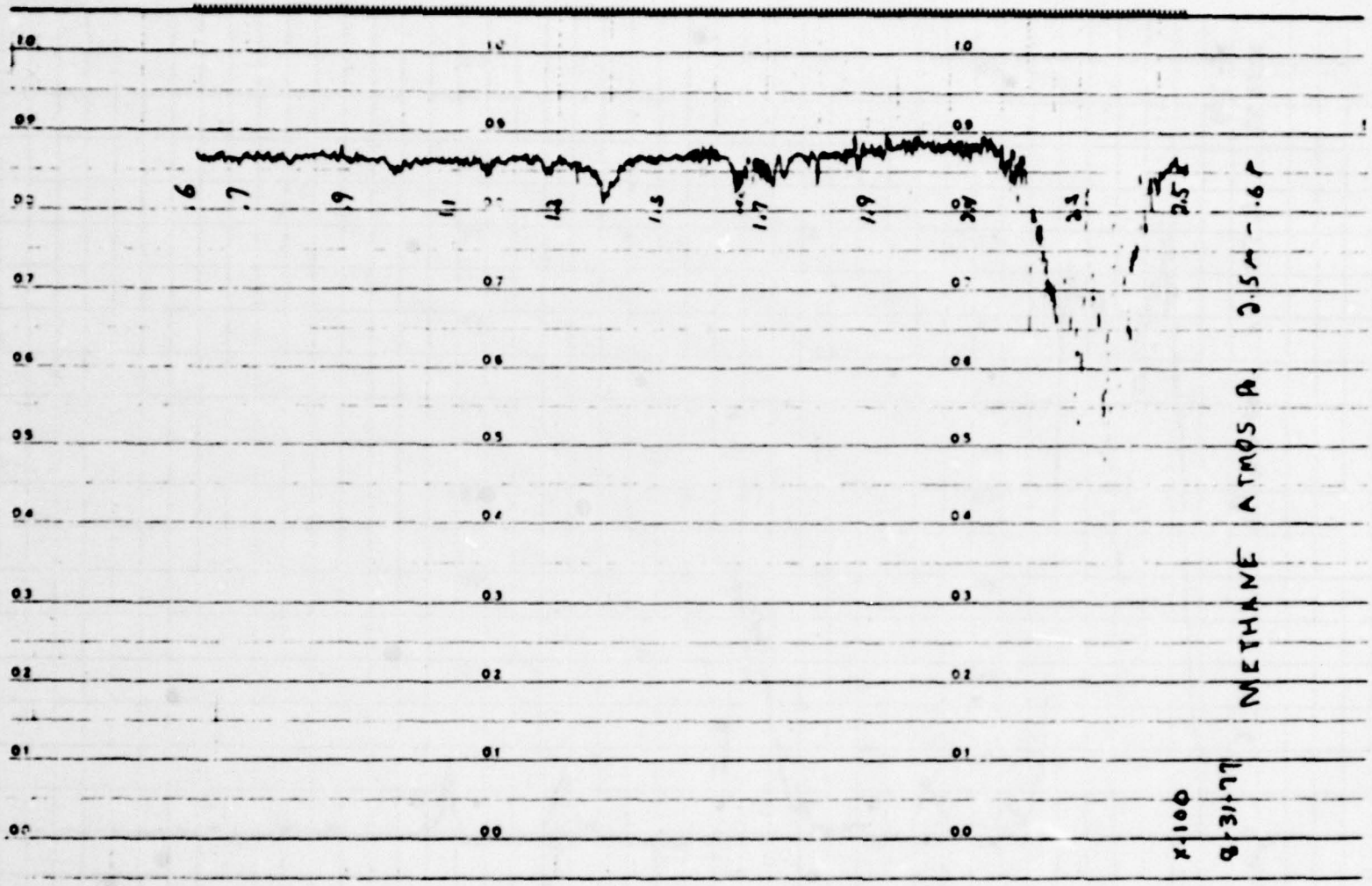

Fig. D-2

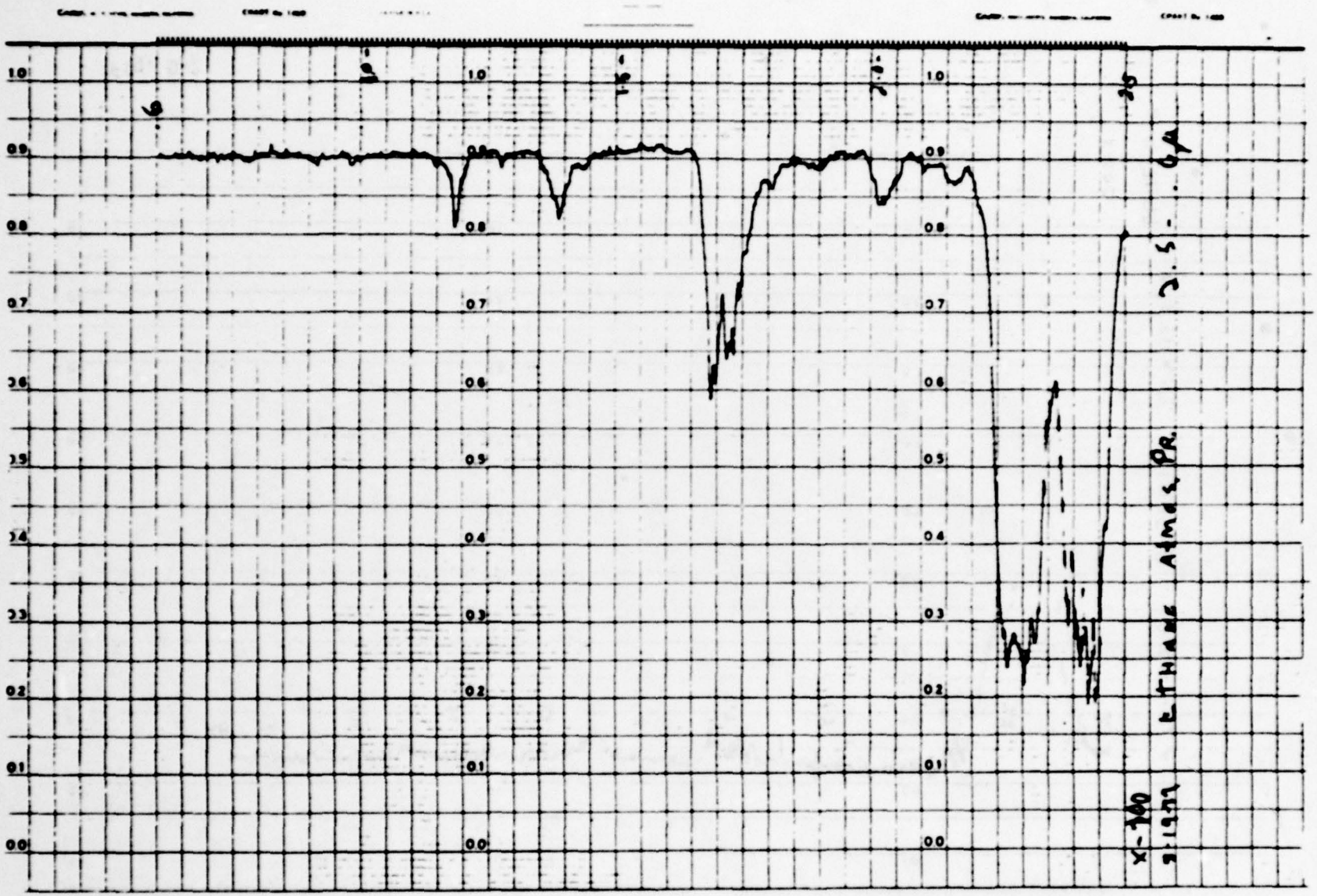

Fig. D-3

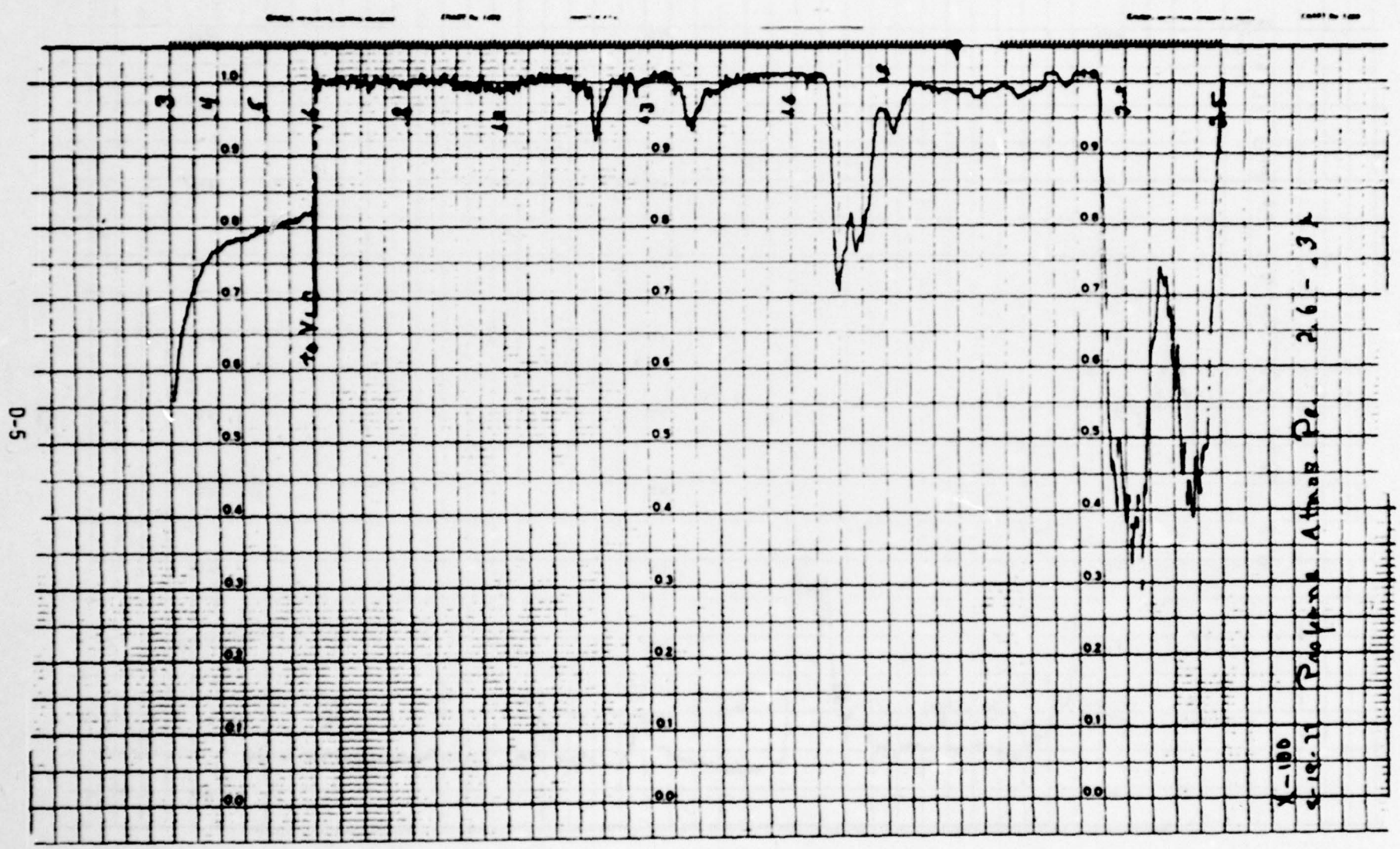

Fig. D-4

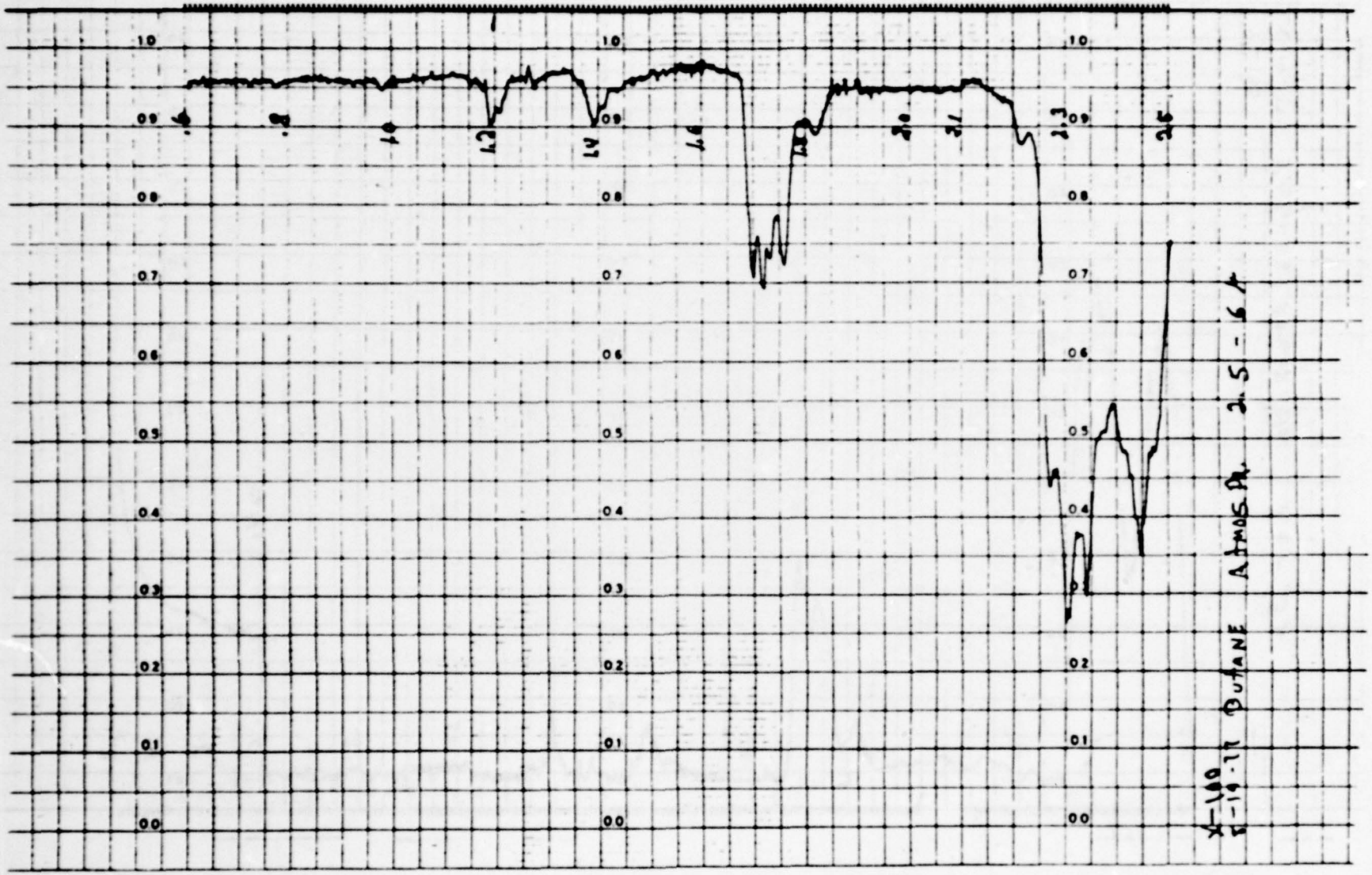

Fig. D-5

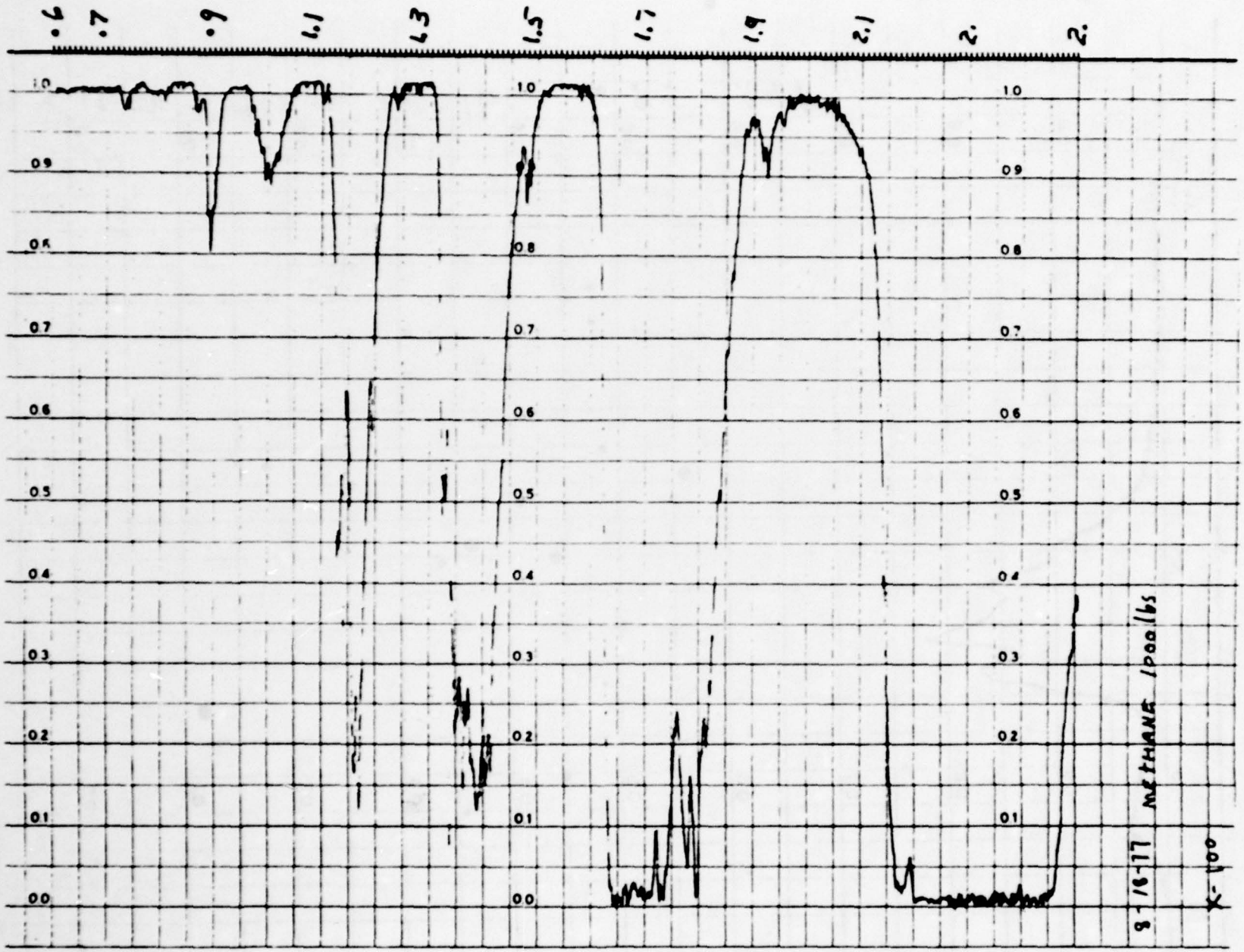
.6
.7
.9
1.1
1.3
1.5
1.7
1.9
2.1
2.
2.
10
09
08
07
06
05
04
03
02
01
00
8-16-77 METHANE 1000/lbs
X-100

Fig. D-6

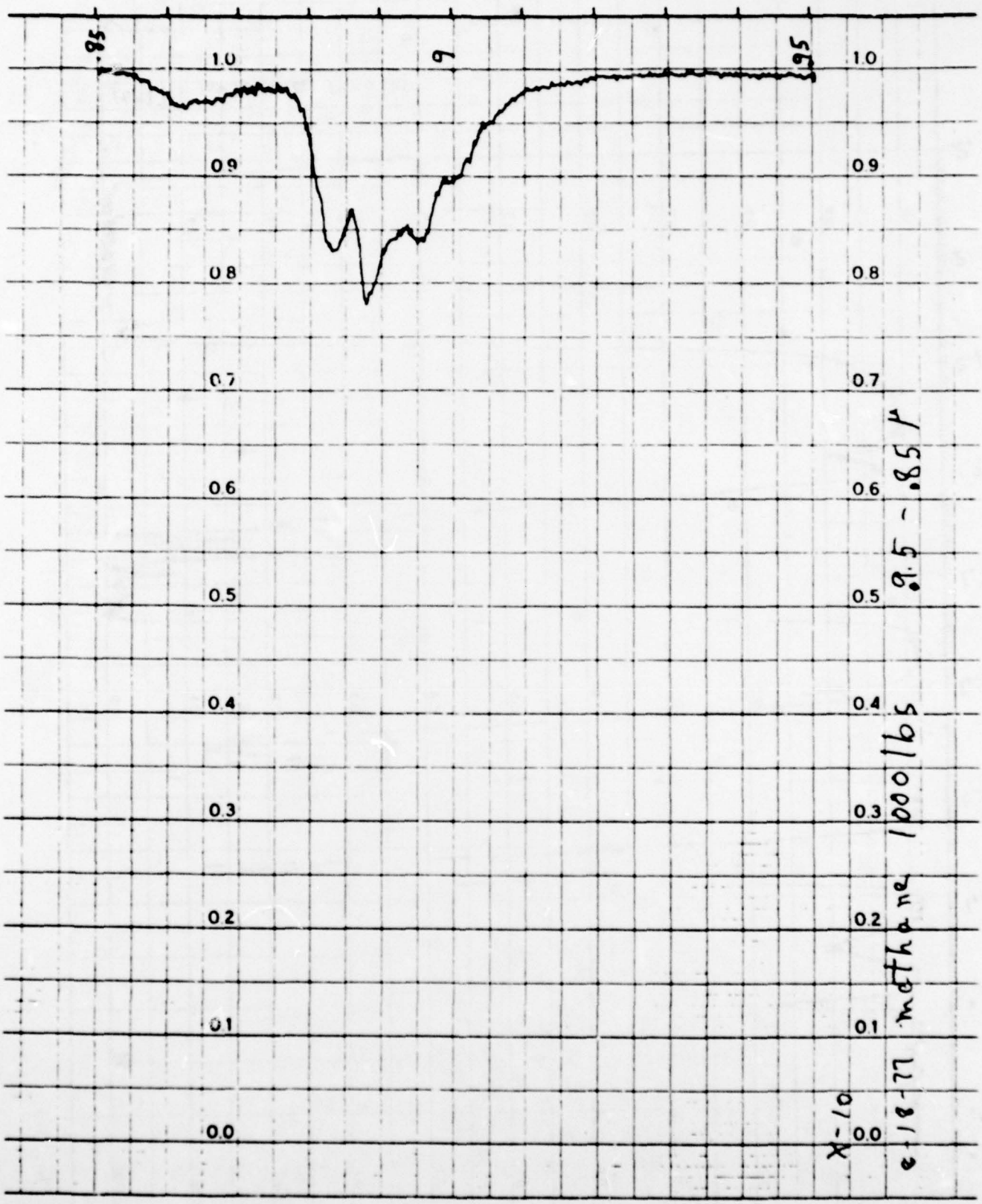
.85
9
.95
1.0
0.9
0.8
0.7
0.6
0.5
0.4
0.3
0.2
0.1
0.0
9.5 - .85 μ
1000 lbs
methane
8-18-77
X-10

Fig. D-7

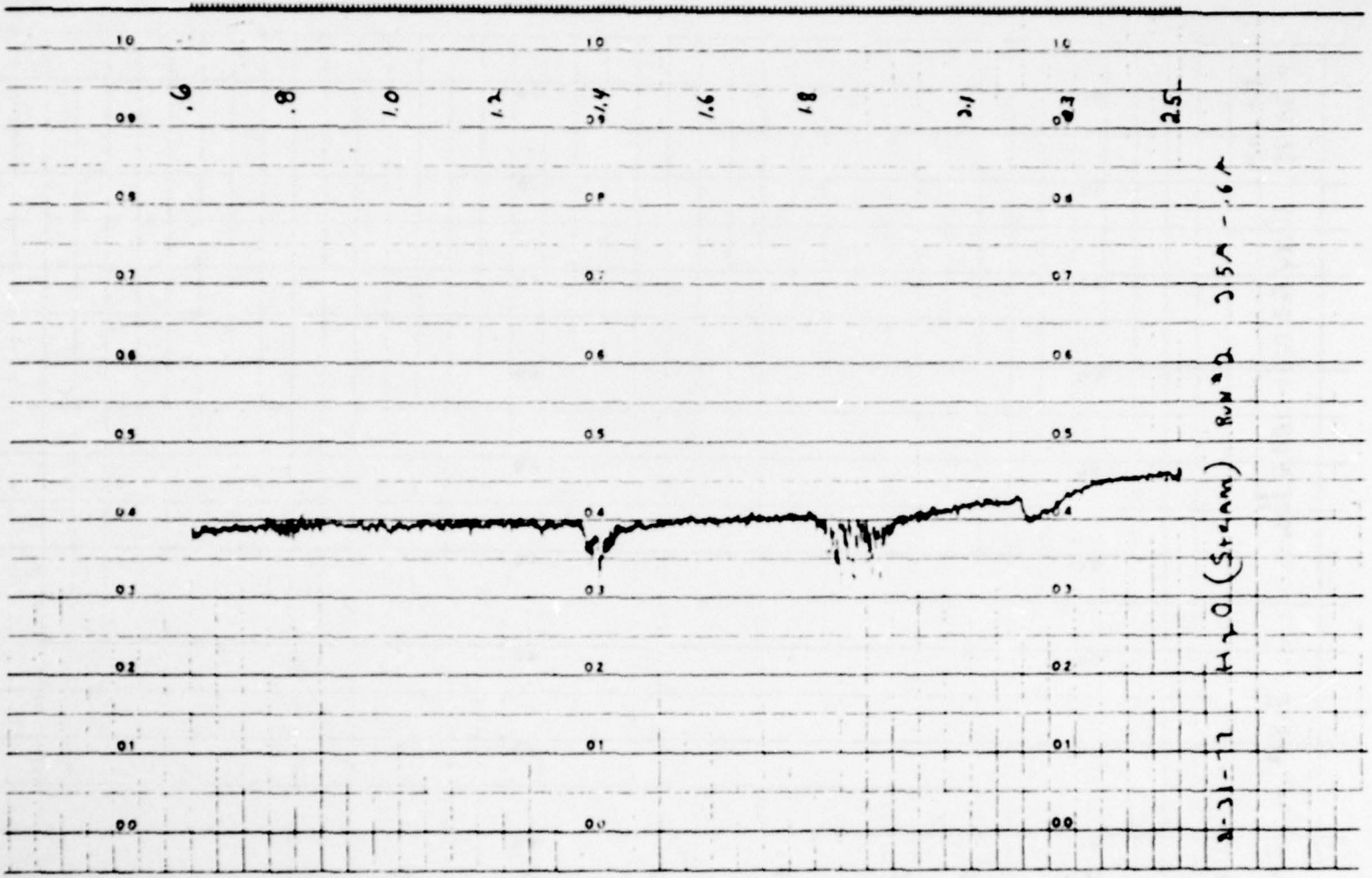

Fig. D-8

Fig. D-9

X - 100
t - 23.77
N2 1000 lbf
2.5A - .6A
2.5
2.0
1.8
1.6
1.4
1.2
1.0
8
6
00
01
02
03
04
05
06
07
08
09
10

Fig. D-10

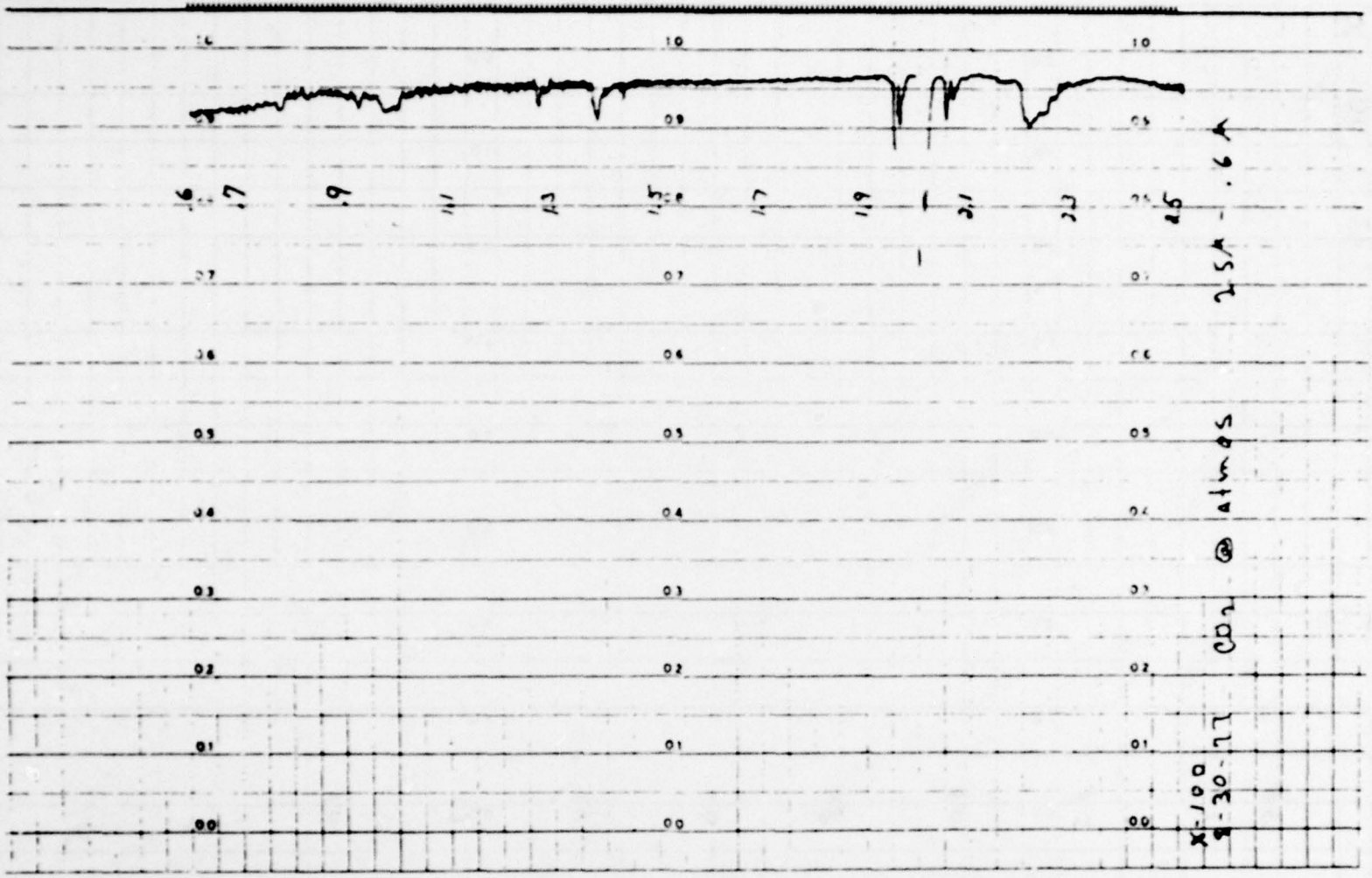

Fig. D-11